Late Paleozoic–Early Triassic magmatism on the western margin of Gondwana: Collahuasi area, Northern Chile

Francisco Munizaga [a], Victor Maksaev [a,*], C.M. Fanning [b], S. Giglio [c], G. Yaxley [d], C.C.G. Tassinari [e]

[a] *Departamento de Geología, Universidad de Chile, Plaza Ercilla 803, Santiago, Chile*
[b] *Research School of Earth Sciences, Australian National University, Canberra, ACT 0200, Australia*
[c] *Compañía Minera Doña Inés de Collahuasi, SCM, Pedro Lagos 1090, Iquique, Chile*
[d] *Research School of Earth Sciences, Australian National University, Canberra ACT 0200, Australia*
[e] *Instituto de Geociencias. Universidade de Sao Paulo, Brazil*

Abstract

The basement in the 'Altiplano' high plateau of the Andes of northern Chile mostly consists of late Paleozoic to Early Triassic felsic igneous rocks (Collahuasi Group) that were emplaced and extruded along the western margin of the Gondwana supercontinent. This igneous suite crops out in the Collahuasi area and forms the backbone of most of the high Andes from latitude 20° to 22°S. Rocks of the Collahuasi Group and correlative formations form an extensive belt of volcanic and subvolcanic rocks throughout the main Andes of Chile, the Frontal Cordillera of Argentina (Choiyoi Group or Choiyoi Granite-Rhyolite Province), and the Eastern Cordillera of Peru.

Thirteen new SHRIMP U–Pb zircon ages from the Collahuasi area document a bimodal timing for magmatism, with a dominant peak at about 300 Ma and a less significant one at 244 Ma. Copper–Mo porphyry mineralization is related to the younger igneous event.

Initial Hf isotopic ratios for the ~300 Ma zircons range from about −2 to +6 indicating that the magmas incorporated components with a significant crustal residence time. The 244 Ma magmas were derived from a less enriched source, with the initial Hf values ranging from +2 to +6, suggestive of a mixture with a more depleted component. Limited whole rock $^{144}Nd/^{143}Nd$ and $^{87}Sr/^{86}Sr$ isotopic ratios further support the likelihood that the Collahuasi Group magmatism incorporated significant older crustal components, or at least a mixture of crustal sources with more and less evolved isotopic signatures.

Keywords: Geochronology; U–Pb; Hf; Sr; and Nd isotope ratios; Andes; Choiyoi; Paleozoic

1. Introduction

An assemblage of mostly felsic volcanic rocks and related porphyritic intrusions are exposed in the Collahuasi area of the 'Altiplano' high plateau of northern Chile (Fig. 1). It forms the basement for Mesozoic and Cenozoic strata and was termed the Collahuasi Formation by Vergara and Thomas (1984). Copper- and gold-bearing veins were mined from the late nineteenth century to the early twentieth century at Collahuasi. Since the 1990s, large-scale exploitation of porphyry copper deposits characterizes the Quebrada Blanca, Rosario, and Ujina open pit mines, which define the present-day Collahuasi mining district. These porphyry copper deposits and the associated hydrothermal alteration zones are Late Eocene to Oligocene in age (Camus, 2003; Masterman et al., 2005), but the surrounding crystalline basement is late Paleozoic to Early Triassic (Table 1). In addition, other low-grade porphyry copper–molybdenum prospects are hosted by the late Paleozoic to Triassic rocks in the region (e.g., Characolla, La Profunda, El Loa, and Los Colorados; Fig. 2). These are part of a regional porphyry copper

* Corresponding author.
E-mail addresses: fmunizag@cec.uchile.cl (F. Munizaga), vmaksaev@cec.uchile.cl (V. Maksaev), Mark.Fanning@anu.edu.au (C.M. Fanning), sfgiglio@collahuasi.cl (S. Giglio), greg.yaxley@anu.edu.au (G. Yaxley), ccgtassi@usp.br (C.C.G. Tassinari).

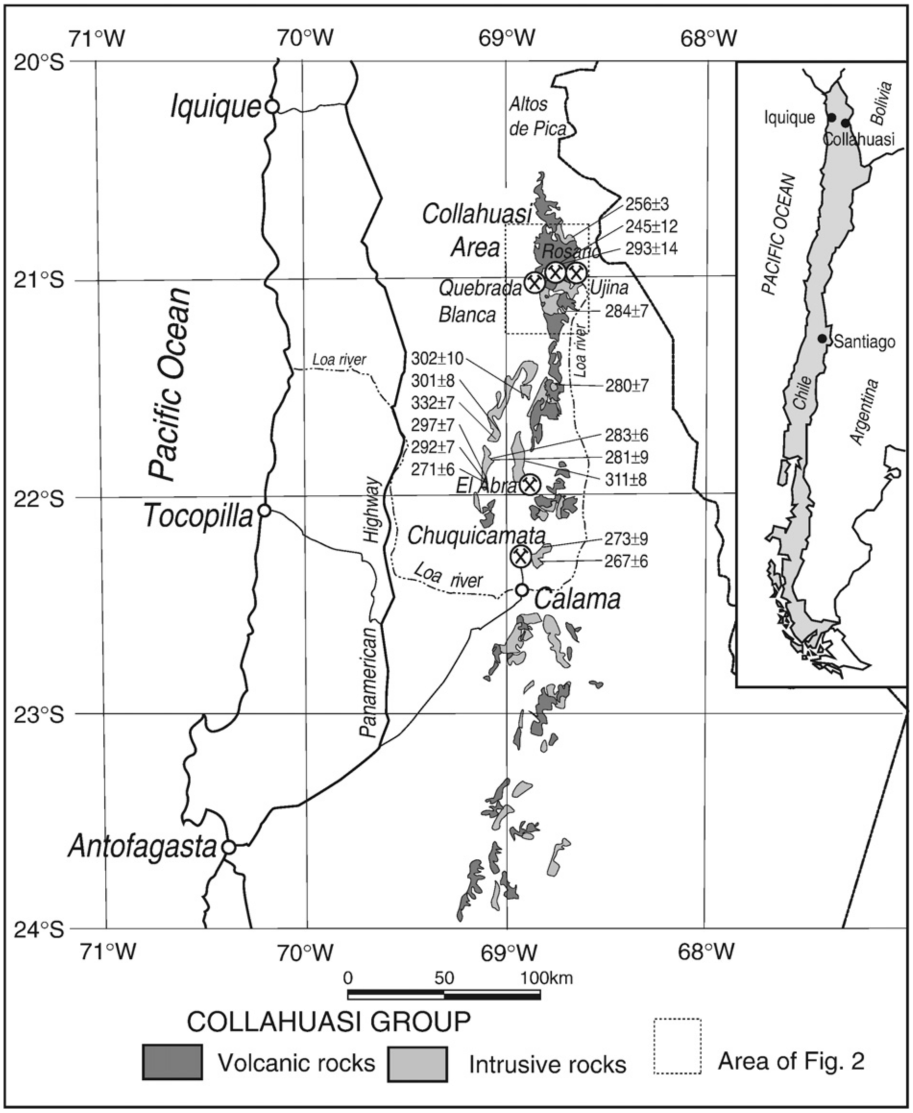

Fig. 1. Location map of the Collahuasi area and geographic distribution of the outcrops of main igneous units of the Collahuasi Group. Previous isotopic ages for granitoids from the region between Collahuasi and Chuquicamata are shown (compiled after Huete et al., 1977; Damm et al., 1986; Lucassen et al., 1999; Tomlinson et al., 2001; Masterman, 2003; see Table 1).

belt that extends from northern Chile to southern Argentina, with K–Ar ages from 290 to ~200 Ma (Camus, 2003; Cornejo et al., 2006).

The basement rocks at Collahuasi are the northernmost exposure in Chile of an extensive belt of late Paleozoic to Early Triassic igneous rocks exposed discontinuously throughout the western Main Andean and eastern Frontal Cordilleras from southern Peru to southern Argentina (Choiyoi Group; e.g., Llambías et al., 1993). Thick volcanic rock sequences are dominant in the Frontal Cordillera of Argentina, whereas large batholiths are widely exposed in Chile, but both rock types are related in space and time along the western margin of Gondwana (e.g., Mpodozis and Kay, 1992). The voluminous felsic rocks have been interpreted as products of crustal anatexis (Breitkreuz and Zeil, 1994; Lucassen et al., 1999; Franz et al., 2006) or as differentiated felsic units of a calk-alkaline subduction-related assemblage, which pre-dates spatially associated felsic anorogenic magmatism (Mpodozis and Kay, 1992).

Accurate dating of the porphyritic intrusions that define these basement rocks in northern Chile has been typically hampered because of regional low-grade metamorphism and/or local overprinting by the Cenozoic hydrothermal alteration. Previous K–Ar dates (e.g., Huete et al., 1977) are mostly equivocal and thus the absolute ages of the felsic igneous rocks are uncertain. We present the first SHRIMP U–Pb zircon data for late Paleozoic to Early Triassic rocks of northern Chile (mostly porphyries of the Collahuasi area), as well as Nd and Sr isotopic ratios and the first Hf isotopic ratios in zircon. This work intends to improve the chronology and the current understanding of late Paleozoic to Early Triassic geological development of the region.

2. Analytical methods

SHRIMP II U–Pb analyses of zircon grains were carried out at the Research School of Earth Sciences, Australian National

Table 1
Compilation of radiometric ages of the region from Collahuasi to Chuquicamata

Sample	Material	Age (Ma±2σ)	Lithology	Latitude S	Longitude W	References
U–Pb ages						
R990259	Zircon	293±14	Rhyodacite	20°58′13″	68°41′52″	Masterman (2003)
R200085	Zircon	245±12	Granodiorite porphyry	20°58′26″	68°41′49″	Masterman (2003)
PZG (D-1)	Zircon	256±3	Granite	20°49′25″	68°42′00″	Damm et al. (1986)
K–Ar ages						
C-350	Biotite	302±10	Granite	21°33′24″	68°54′49″	Huete et al. (1977)
QBB-310	Biotite	297±7	Granodiorite	21°55′52″	69°05′47″	Tomlinson et al. (2001)
QBB-306	Biotite	292±7	Granite	21°57′12″	69°05′35″	Tomlinson et al. (2001)
QBB-284	Biotite	271±6	Granite	21°56′56″	69°07′26″	Tomlinson et al. (2001)
4/417	Biotite	301±8	Granite	21°42′58″	69°01′51″	Lucassen et al. (1999)
Apr-36	Biotite	332±7	Granite	21°45′21″	69°02′81″	Lucassen et al. (1999)
3/299	Biotite	283±6	Granite	21°51′03″	69°06′00″	Lucassen et al. (1999)
3/300	Hornblende	281±9	Diorite	21°51′03″	69°05′00″	Lucassen et al. (1999)
QT-140	Hornblende	273±9	Diorite	22°15′33″	68°51′19″	Tomlinson et al. (2001)
QT-108	Biotite	267±6	Diorite	22°19′00″	68°50′45″	Tomlinson et al. (2001)
D-2	Biotite	311±8	Granite	21°51′30″	68°55′30″	Huete et al. (1977)
QB-92	Biotite	284±7	Granodiorite	21°09′42″	68°42′57″	Tomlinson et al. (2001)
QB-66	Biotite	280±7	Granodiorite	21°26′21″	68°46′38″	Tomlinson et al. (2001)

Note: The table includes only K–Ar ages obtained in fresh mineral phases with normal K content.

University. A detailed description of procedures is given in Appendix A, and the data tabulations for all thirteen samples in Appendix B. A summary of the U–Pb zircon age determinations is given in Table 2.

Rubidium–Sr and Sm–Nd isotopic analyses of four samples of volcanic rocks were carried out at the Geochronological Research Center of the University of Sao Paulo, Brazil. The isotopic data are given in Table 3 and description of analytical procedures is given in Appendix A.

Laser ablation multi-collector inductively coupled plasma mass spectrometry Lu–Hf isotopic analyses were carried out on the same zircon grains used for the U–Pb analyses. A detailed description of procedures is given in Appendix A. The isotopic data are given in Table 4.

3. Late Paleozoic to Triassic magmatism

The late Paleozoic–early Mesozoic magmatism is a significant, but not well understood geological event, which has been recognized along much of the length of western South America (e.g., Vaughan and Pankhurst, 2007). The late Paleozoic to Triassic igneous units along the high Andes of Chile and the Argentinean Frontal Cordillera are commonly known by a variety of names. Rolleri and Criado-Roque (1970) used the name Choiyoi for late Paleozoic to Triassic felsic and intermediate units outcropping in the Argentinean Frontal Cordillera, and this name has been widely used to refer to Permo-Triassic magmatism in both countries. The Choiyoi Group is comprised of volcano-plutonic complexes that represent magmatism along the western border of Gondwana (Llambías and Sato, 1990; Sato and Llambías, 1993; Mpodozis and Kay, 1992; Strazzere et al., 2006). These rocks are included in the Choiyoi Granite-Rhyolite Province of Mpodozis and Kay (1992), which extends for 2500 km from the Collahuasi area in northern Chile to Neuquén and the northern Patagonian Andes in southern Argentina, and is also correlated with the Mitu Group of southern Peru (Carlier et al., 1982).

The volcanic components of the late Paleozoic to Triassic magmatism are not exposed from about latitude 25°S to 33°S, but granitic and granodioritic batholiths of the same episode outcrop along the present-day high Andes (Marinovic et al., 1995; Nasi et al., 1985; Mpodozis and Kay, 1990, 1992). Martin et al. (1999) have identified at least three discrete intrusive units in this region according to U–Pb and K–Ar data: biotite granites (280–270 Ma), silica-rich leucocratic granites and rhyolitic porphyries (242–238 Ma), and rhyolitic porphyries, domes and mafic intrusions (221–200) Ma. The geochemical characteristics of the intrusions are consistent with initial subduction-related magmatism, followed by extensive crustal melting (Mpodozis and Kay, 1992).

Permian–Triassic alkaline to calc-alkaline batholiths and stocks occur in the Eastern Cordillera of Peru and, together with the alkaline volcanic rocks of the Mitu Group, they form a Permian–Triassic magmatic belt over a length of more than 1000 km in a NNW–SSE direction in the Eastern Cordillera (Carlier et al., 1982 and references therein). The volcanism and plutonism appear to be related to crustal melting. Uranium–Pb zircon data indicate an age of 336 to 325 Ma for the Pataz batholith (Miskovic and Schaltegger, 2006; Schaltegger et al., 2006). Mississippian I-type metaluminous to peraluminous granitoids are chiefly restricted to the segment of the Eastern Cordillera north of 11°S, with dates on plutons at Huacapistana (310 Ma), Hualluniyocc (325 Ma), and Utcuyacu (307 Ma) (Chew et al., 2007). Permian to Early Triassic S- to A-type granitoids in central and southern Peru are comagmatic with lavas of the Mitu Group, all of which are post-tectonic suites and include U–Pb and Rb–Sr ages of 250–240 Ma for the San Ramón granite (Capdevila et al., 1977; Lancelot et al. 1978). Additional magmatic activity in the Eastern Cordillera of Peru

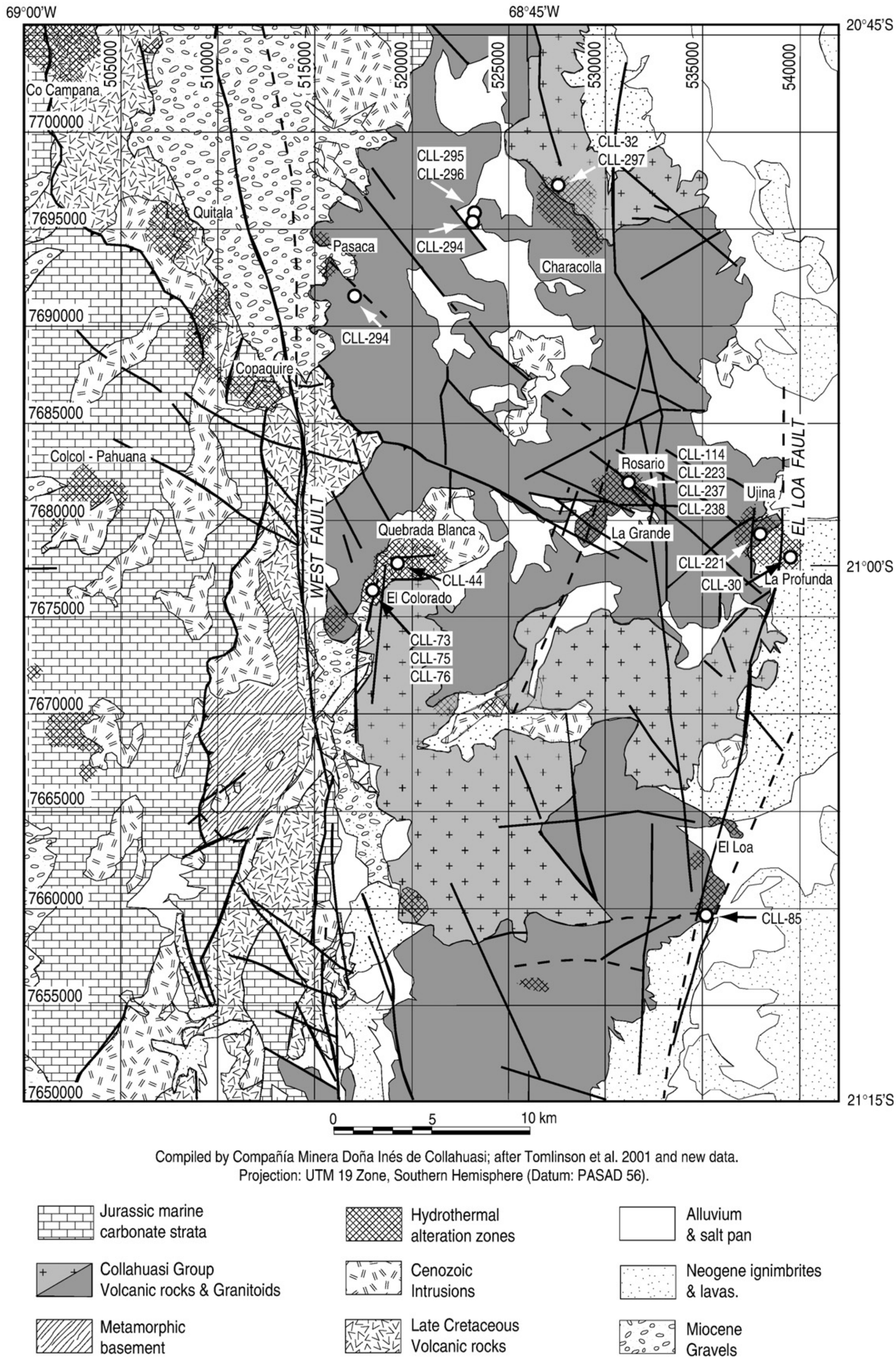

Fig. 2. Regional geological map of the Collahuasi area showing sample localities.

Table 2
Summary of the new SHRIMP zircon U–Pb ages and sample location

Sample	Weighted mean $^{206}Pb/^{238}U$ age (Ma±2σ)	Rock type	Location	Comments
CLL-44	303.2±2.0	Granitic porphyry	Quebrada Blanca Mine 21°00′14″S – 68°48′50″W DDH 59; 106–107 m	Weighted mean for 19 of 23 analyzed spots; excluded 3 with interpreted radiogenic Pb loss, and one inherited at ~750 Ma.
CLL-73	292.7±1.9	Granitic porphyry	Los Colorados Prospect 21°01′41″S – 68°50′33″W Surface	Weighted mean for 20 of 20 analyzed spots.
CLL-75	307.9±2.8	Rhyolitic porphyry	Los Colorados Prospect 21°01′57″S – 68°50′40″W Surface	Weighted mean for 16 of 20 analyzed spots; excluded 4 with interpreted radiogenic Pb loss
CLL-76	298.8±2.2	Dacite	Los Colorados Prospect 21°01′53″S – 68°50′54″W Surface	Weighted mean for 16 of 18 analyzed spots; excluded 2 with interpreted radiogenic Pb loss
CLL-85	297.6±2.4	Rhyolitic porphyry	El Loa Prospect 21°09′42″S – 68°39′36″W Surface	Weighted mean for 17 of 20 analyzed spots; excluded 3 with interpreted radiogenic Pb loss
CLL-114	304.6±3.2	Rhyolitic porphyry	Rosario Mine 20°58′19″S – 68°42′13″W C-177; 632 m	Weighted mean for 6 spots.
CLL-221	296.9±4.3	Dacite porphyry	Ujina Mine 20°59′08″S – 68°38′03″W Open pit	Weighted mean for 8 of 11 analyzed spots; excluded 2 with interpreted radiogenic Pb loss, and one inherited at ~318 Ma.
CLL-223	298.3±2.1	Rhyolitic porphyry	Rosario Mine 20°57′56″S – 68°42′11″W Open pit	Weighted mean for 16 of 20 analyzed spots; excluded 3 with interpreted radiogenic Pb loss, and one older at ~310 Ma.
CLL-237	303.9±3.0	Rhyolitic porphyry	Rosario Mine 20°58′09″S – 68°42′17″W C-322; 497 m	Weighted mean for all 6 analyzed spots.
CLL-238	308.5±2.2	Rhyolitic porphyry	Rosario Mine 20°58′19″S – 68°42′13″W C-177; 573 m	Weighted mean for 17 of 20 analyzed spots; excluded 3 with interpreted radiogenic Pb loss.
CLL-30	244.8±2.5	Dacite porphyry	La Profunda Prospect 21°00′19″S – 68°36′43″W PUC-611; 421 m	Enrichment in common Pb for many analyses. Weighted mean for 27 of 31 spots; excluded 4 spots with interpreted radiogenic Pb loss
CLL-297	248.7±3.3	Granite porphyry	Characolla Prospect 20°50′37″S – 68°44′59″W Surface	Age estimate for only 3 of 4 grains analyzed.
CLL-32	243.2±2.1	Granite porphyry	Characolla Prospect 20°50′37″S – 68°44′59″W RLC-01; 171 m	Enrichment in common Pb for most analyses. Weighted mean for 18 of 20 analyzed spots; excluded one with interpreted radiogenic Pb loss, and one older at ~305 Ma.

included eruption of progressively more alkaline lavas of the Mitu Group and A-type plutonism, which peaked between 216–205 Ma (Miskovic and Schaltegger, 2006).

SHRIMP zircon U–Pb and $^{40}Ar/^{39}Ar$, together with other geochronological data allowed Vinasco et al. (2006) to conclude that discrete magmatic events characterized the Permian and

Table 3
Rb–Sr and Sm–Nd isotopic data

Sample	Rb (ppm)	Sr (ppm)	$^{87}Rb/^{86}Sr$	$^{87}Sr/^{86}Sr$	$^{87}Sr/^{86}Sr$ (300 Ma)	Lithology	Lat. S	Long. W	Altitude (m)
CLL-293	156.7	44.4	10.231	0.72076	0.67780	Rhyolite	20°52′29″	68°50′04″	4309
CLL-294	175.5	429.9	1.181	0.71079	0.70575	Andesite	20°50′33″	68°46′21″	4251
CLL-295	192.8	430.4	1.297	0.71106	0.70552	Andesite	20°50′31″	68°46′22″	4260
CLL-296	2.1	95.0	0.065	0.70639	0.70611	Andesite	20°50′32″	68°46′21″	4257

Sample	Sm (ppm)	Nd (ppm)	$^{147}Sm/^{144}Nd$	$^{143}Nd/^{144}Nd$	Uncertainty	$^{143}Nd/^{144}Nd$ (300 Ma)	ε_{Nd} (300 Ma)	T DM (Ma) 2nd Stage
CLL-293	5.568	26.627	0.1264	0.512449	0.000012	0.512201	−1.46	1115
CLL-294	5.310	22.764	0.1410	0.512461	0.000009	0.512184	−1.79	1139
CLL-295	5.990	25.759	0.1406	0.512472	0.000011	0.512196	−1.56	1122
CLL-296	4.322	16.981	0.1539	0.512478	0.000013	0.512176	−1.95	1152

Table 4
Lu–Hf in zircon isotopic data

Sample	Grain	Spot	$^{176}Hf/^{177}Hf$	±2σ	$^{176}Lu/^{177}Hf$	±2σ	U–Pb age (T1)	ε_{Hf} (0)	±2σ	ε_{Hf} (T1)	T DM (2)
CLL-30	5	1	0.282741	0.000022	0.000792	0.000012	245	−1.09	0.79	4.16	959
	8	1	0.28273	0.000024	0.000813	0.000014	245	−1.49	0.86	3.76	979
	14	1	0.282777	0.000022	0.000756	0.000023	245	0.17	0.76	5.44	870
	18	1	0.282754	0.000023	0.001038	0.00004	245	−0.63	0.8	4.58	928
	23	1	0.282743	0.000023	0.000993	0.000039	245	−1.03	0.83	4.19	953
	24	1	0.282735	0.000026	0.001203	0.000035	245	−1.29	0.9	3.9	966
	31	1	0.28276	0.000027	0.000854	0.000017	245	−0.41	0.96	4.83	907
	34	1	0.28275	0.000026	0.000852	0.00002	245	−0.79	0.92	4.45	928
CLL-32	1	1	0.282785	0.000028	0.001512	0.000023	243	0.44	0.98	5.54	862
	3	1	0.282757	0.000021	0.001885	0.000039	243	−0.54	0.76	4.49	929
	5	1	0.282694	0.000031	0.002489	0.000097	243	−2.77	1.1	2.17	1077
	12	1	0.282599	0.000023	0.000553	0.000004	305	−6.12	0.82	0.47	1234
	11	1	0.282746	0.000022	0.001151	0.000023	243	−0.92	0.77	4.23	949
	10	1	0.282782	0.000026	0.001783	0.000034	243	0.37	0.91	5.43	866
	14	1	0.282714	0.000021	0.001176	0.000022	243	−2.06	0.75	3.09	1017
	18	1	0.282731	0.000023	0.001243	0.00002	243	−1.45	0.82	3.69	978
CLL-44	2	1	0.282729	0.000031	0.00256	0.000107	303	−1.52	1.1	4.63	968
	4	1	0.28268	0.000025	0.000861	0.000013	303	−3.24	0.89	3.25	1055
	5	1	0.282665	0.000027	0.003532	0.000212	303	−3.79	0.94	2.17	1124
	10	1	0.282656	0.000031	0.002588	0.000049	303	−4.1	1.11	2.05	1132
	12	1	0.282693	0.000025	0.000847	0.000017	303	−2.78	0.89	3.72	1026
	13	1	0.282725	0.000025	0.001043	0.000007	303	−1.66	0.89	4.8	957
	16	1	0.282572	0.00002	0.001233	0.000008	303	−7.07	0.7	−0.66	1304
	19	1	0.282688	0.00003	0.000938	0.000014	303	−2.97	1.07	3.5	1039
CLL-73	1	1	0.282693	0.000029	0.003825	0.000033	293	−2.79	1.03	2.91	1069
	2	1	0.282742	0.000031	0.002561	0.000107	293	−1.06	1.1	4.89	943
	5	1	0.282686	0.000015	0.001249	0.000088	293	−3.05	0.52	3.15	1054
	6	1	0.282704	0.000015	0.001284	0.000125	293	−2.41	0.54	3.78	1014
	10	1	0.282692	0.000017	0.002317	0.000033	293	−2.82	0.6	3.17	1053
CLL-75	3	1	0.282607	0.000036	0.001289	0.000057	308	−5.84	1.27	0.67	1224
	7	1	0.282625	0.00003	0.001158	0.000005	308	−5.2	1.05	1.33	1181
	8	1	0.282549	0.000036	0.001675	0.000053	308	−7.9	1.27	−1.47	1360
	10	1	0.282601	0.000031	0.001837	0.000063	308	−6.05	1.1	0.34	1244
	11	1	0.282559	0.000038	0.001234	0.000042	308	−7.52	1.33	−1	1330
CLL-76	1	1	0.282686	0.000021	0.000442	0.00004	299	−3.05	0.74	3.44	1040
	5	1	0.282696	0.000033	0.001747	0.000082	299	−2.69	1.17	3.54	1034
	9	1	0.28277	0.000036	0.002918	0.000134	299	−0.06	1.26	5.94	881
	10	1	0.282728	0.00004	0.006285	0.000045	299	−1.54	1.43	3.79	1018
	1	1	0.282656	0.000029	0.001517	0.000038	298	−4.1	1.03	2.16	1121
	2	1	0.282606	0.000024	0.000845	0.000013	298	−5.88	0.85	0.51	1226
	3	1	0.282592	0.000029	0.001363	0.000041	298	−6.38	1.02	−0.1	1265
	5	1	0.282612	0.000026	0.000871	0.000036	298	−5.67	0.9	0.71	1214
	7	1	0.282572	0.000026	0.0012	0.000031	298	−7.07	0.92	−0.76	1306
CLL-238	20	1	0.282555	0.000017	0.001252	0.000006	309	−7.66	0.61	−1.12	1338
	16	1	0.282542	0.000036	0.001919	0.000074	309	−8.14	1.28	−1.74	1377
	10	1	0.28259	0.000028	0.001656	0.000072	309	−6.43	0.98	0.02	1265
	8	1	0.282584	0.000024	0.001229	0.000034	309	−6.65	0.83	−0.11	1274
	6	1	0.282606	0.000024	0.001156	0.000055	309	−5.88	0.84	0.68	1224
	11	1	0.282582	0.000024	0.001169	0.000043	309	−6.73	0.84	−0.17	1278
CLL-297	1	1	0.282748	0.00002	0.001409	0.000038	250	−0.84	0.72	4.42	939
	3	1	0.282747	0.000021	0.001436	0.00002	250	−0.89	0.72	4.37	943
	4	1	0.282722	0.000021	0.001463	0.000043	250	−1.78	0.73	3.47	1000

Triassic Colombian Andes at ca. 300–270 Ma, 250 Ma, and 230 Ma. These were interpreted to represent late-tectonic, extension-related magmatism.

4. The Collahuasi Group

An assemblage of felsic volcanic rocks and associated porphyry intrusions that mainly comprise the late Paleozoic to Triassic basement in the Chilean Altiplano in the Collahuasi area was originally defined as the Collahuasi Formation (Vergara, 1978; Vergara and Thomas, 1984). We refer to this unit as the Collahuasi Group because it displays a complex succession of intermediate to felsic lava flows, pyroclastic and sedimentary rocks, ignimbrites, sub-volcanic bodies, and domes. This complex combination of facies and the absence of detailed mapping hinder definition of an accurate stratigraphy. The Collahuasi Group is correlative with a number of other Late Carboniferous to Triassic basement formations along the

Domeyko Cordillera and the Main Andes in northern Chile. These include the Quipisca Formation at 20°S (Galli 1968), the La Tabla Formation between 24°S and 27°S (García 1967; Marinovic et al. 1995; Cornejo et al. 1998, 2006; Tomlinson et al. 1999), the Tuina Formation (Marinovic and Lahsen 1984), the Agua Dulce Formation (García 1967; Marinovic and Lahsen 1984), the Pantanoso Formation in the Copiapó region at 27–28°S (Mercado 1982; Iriarte et al. 1996), the lower part of the Pastos Blancos Group (Martin et al. 1999), and the Peine Formation (i.e., Marinovic and García 1999).

The base of the Collahuasi Group is not exposed, but it is thought to unconformably overlie early Paleozoic intrusive rocks emplaced into metamorphic rocks (Sierra de Moreno Schists; Skarmeta and Marinovic, 1981) that are part of the Arequipa–Antofalla craton (Ramos, 1988; Casquet et al., 2007), and Devonian–Carboniferous sedimentary rocks that outcrop 50 km southeast of Collahuasi (Tomlinson et al., 2001). In turn, rocks of the Collahuasi Group are unconformably covered by Jurassic marine carbonate rocks (Quehuita Formation; Vergara and Thomas, 1984), as well as locally Middle to Late Triassic sedimentary and volcanic rocks (Tomlinson et al., 2001).

Rocks of the Collahuasi Group are exposed along a 200-km-long, north–south belt bounded by the West and the El Loa regional faults, which are part of the north–south Domeyko strike-slip fault system (Fig. 2; Maksaev, 1990; Boric et al., 1990). The Rio Loa fault has been recognized immediately east of the Ujina porphyry copper deposit and extends south along the headwaters of the Loa River, but is mostly covered by extensive late Miocene ignimbrite strata (Bisso et al., 1998). The northern termination of the Collahuasi Group is poorly defined because the unit is buried beneath the middle Miocene Huasco Ignimbrite (Vergara and Thomas, 1984). A crustal block of predominantly Paleozoic basement, which is bounded by the West and the Rio Loa faults, is inferred to have been uplifted during the late Eocene Incaic orogeny (Masterman, 2003). This uplift is recorded by apatite fission track ages of 41 to 34 Ma for the basement rocks at Collahuasi (Maksaev et al., 2006).

Vergara and Thomas, (1984) identified three members of the Collahuasi Group: the lower member is comprised of dacite and rhyolite with intercalated sandstone and limestone lenses, a middle member is mainly composed of andesitic rocks, and an upper member is composed mostly of dacite and rhyolite. However, on a regional scale, the volcanic rocks of the Collahuasi Group have significant lateral lithological variation that is probably due to association with different volcanic centers. The relative stratigraphic position of the outcropping volcanic rocks is not always clear, due to fault displacements and lack of stratigraphic marker horizons. Thus regional mapping has simply defined units based on the dominant lithologies. The general description presented here follows that of Tomlinson et al. (2001).

The lower member of rhyolite and dacite form a succession with a massive appearance and a maximum thickness of 2500 m. The sequence is mostly composed of 20- to 100-m-thick dacitic and rhyolitic flows and tuffs, tuffaceous breccias, and ignimbrite horizons. These extrusive rocks show parallel flow-banding and identifiable contacts between successive flows. Frequently, they grade laterally into intrusive porphyry facies, with crosscutting subvertical contacts and local sub-vertical flow-banding. For this reason, delimitation of the intrusive facies is difficult during field mapping. Lithological characteristics indicate that the unit represents effusive dome and flow-dome complexes, and thick viscous lava flows, with porphyritic intrusions that likely were their feeder conduits. A finely stratified sedimentary succession, about 150-m-thick, is intercalated with the igneous rocks in the Collahuasi area. Individual beds vary from a few centimeters to a number of meters in thickness, and are composed of gray limestones, laminated siliceous levels (chert) with lesser calcite, and green and red sandstone strata.

The middle member is composed of andesite lavas, but also basalt flows (49–56% SiO_2; Tomlinson et al., 2001), forming a massive 1800-m-thick unit at Collahuasi; stratification is only apparent when tuffaceous levels are intercalated. The unit is mainly composed of dark volcanic and volcaniclastic rocks. There are a number of volcanic rock textures, ranging from porphyritic andesitic-basaltic rocks with large plagioclase phenocrysts, which are as much as 3-cm-long, to fine-grained aphanitic rocks.

The upper member of rhyolite and dacite forms a succession with a maximum exposed thickness of 1100 m. It is formed mainly by massive dacite and rhyolite beds, with andesite intercalated in the uppermost part of the succession.

Sub-volcanic stocks of rhyolite porphyry form an integral part of the Collahuasi Group. These are pink to purple, coarse-grained to porphyritic rocks with abundant quartz augen, which either have sharp contacts or are transitional to flow-domes and silicic lava flows. The rocks are biotite and/or hornblende rhyolite with phenocrysts of K-feldspar, plagioclase, and embayed quartz that are as much as 5 mm in diameter; the groundmass is composed of a microcrystalline (recrystallized) aggregate of quartz and feldspar. Typically, the mafic minerals are replaced by chlorite, epidote, calcite, and opaque minerals, whereas the feldspars are partly altered to sericite and clay minerals.

Extensive equigranular granitoid batholiths, with a wide range of composition from syenogranite to diorite, are exposed from Altos de Pica to Chuquicamata (Fig. 1). They are emplaced into the late Paleozoic felsic volcanic strata. Although distinct intrusions, these batholiths are temporally associated with rocks of the Collahuasi Group and collectively form the basement in the region. Biotite and amphibole K–Ar ages, and a few U–Pb zircon determinations for the intrusions, range from 332 to 245 Ma (Huete et al., 1977; Damm et al., 1986; Lucassen et al., 1999; Tomlinson et al., 2001; and Masterman, 2003) (Table 1; Fig. 1).

5. Geochronology

Samples of basement rocks in the Collahuasi area were obtained from the Quebrada Blanca, Rosario, and Ujina mines and from the Los Colorados, Characolla, La Profunda, and El Loa prospects. A summary of the thirteen new SHRIMP U–Pb zircon age determinations is presented in Table 2. The respective Tera and Wasserburg concordia plots and U–Pb age relative probability plots are shown in Figs. 3–6, whereas the full analytical data are given in Appendix B.

Nine felsic porphyries have SHRIMP U–Pb zircon ages in the range 308.5±2.2 Ma to 292.7±1.9 M. These data are derived from a weighted mean of $^{206}Pb/^{238}U$ ages for the analyses of zoned igneous zircon as evidenced by cathodoluminescence imaging of sectioned grains. A dacite from a dome at El Colorado has an U–Pb age of 298.8±2.2 Ma (Table 2). On a relative probability plot for all thirteen U–Pb age determinations (Fig. 7), these ten felsic volcanic rocks form a major

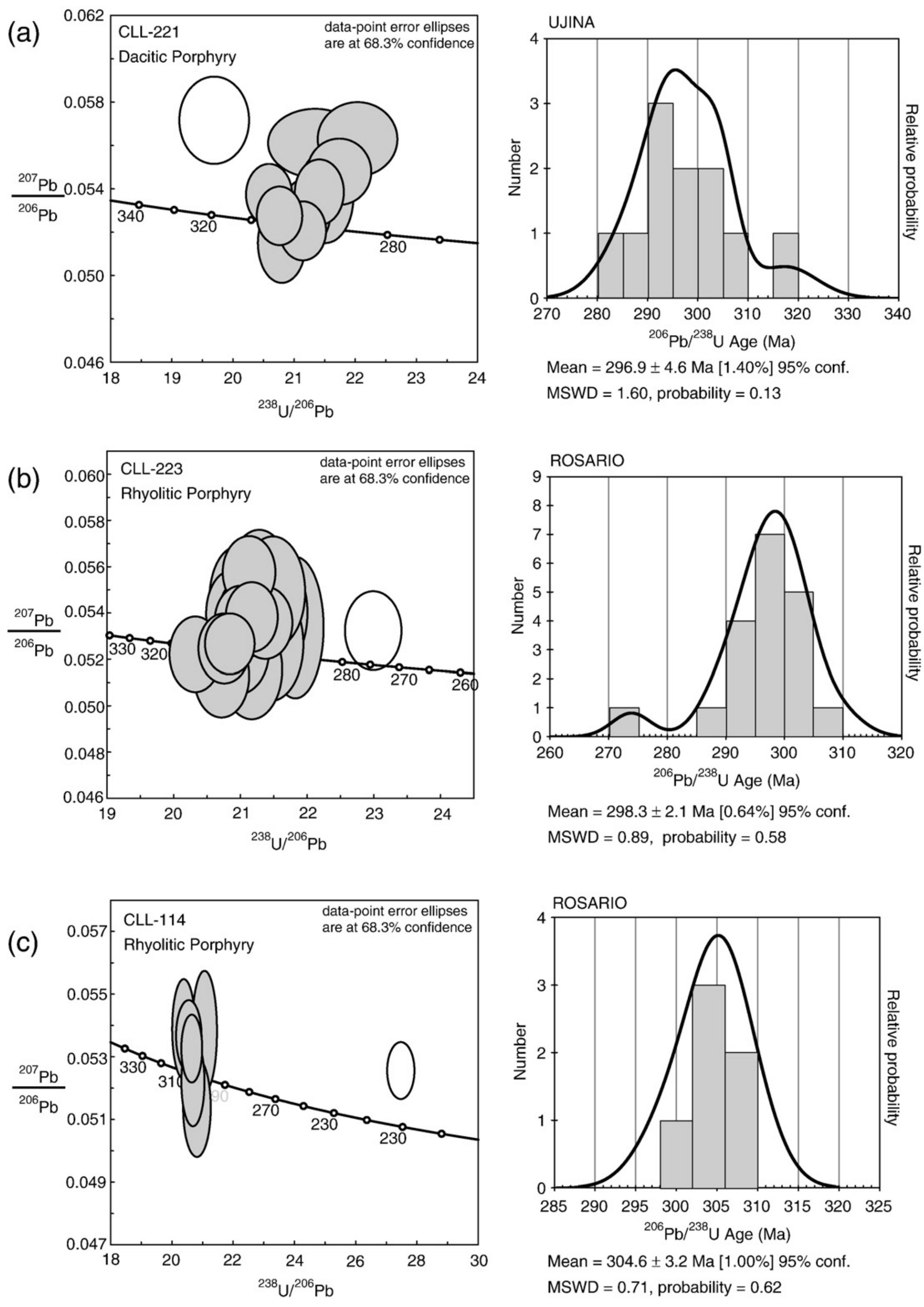

Fig. 3. Tera-Wasserburg concordia plot and probability density plot with stacked histogram of SHRIMP U–Pb age data for: (a) dacitic porphyry of Ujina (CLL-21); (b) rhyolitic porphyry of Rosario (CLL-223); and (c) rhyolitic porphyry of Rosario (CLL-114).

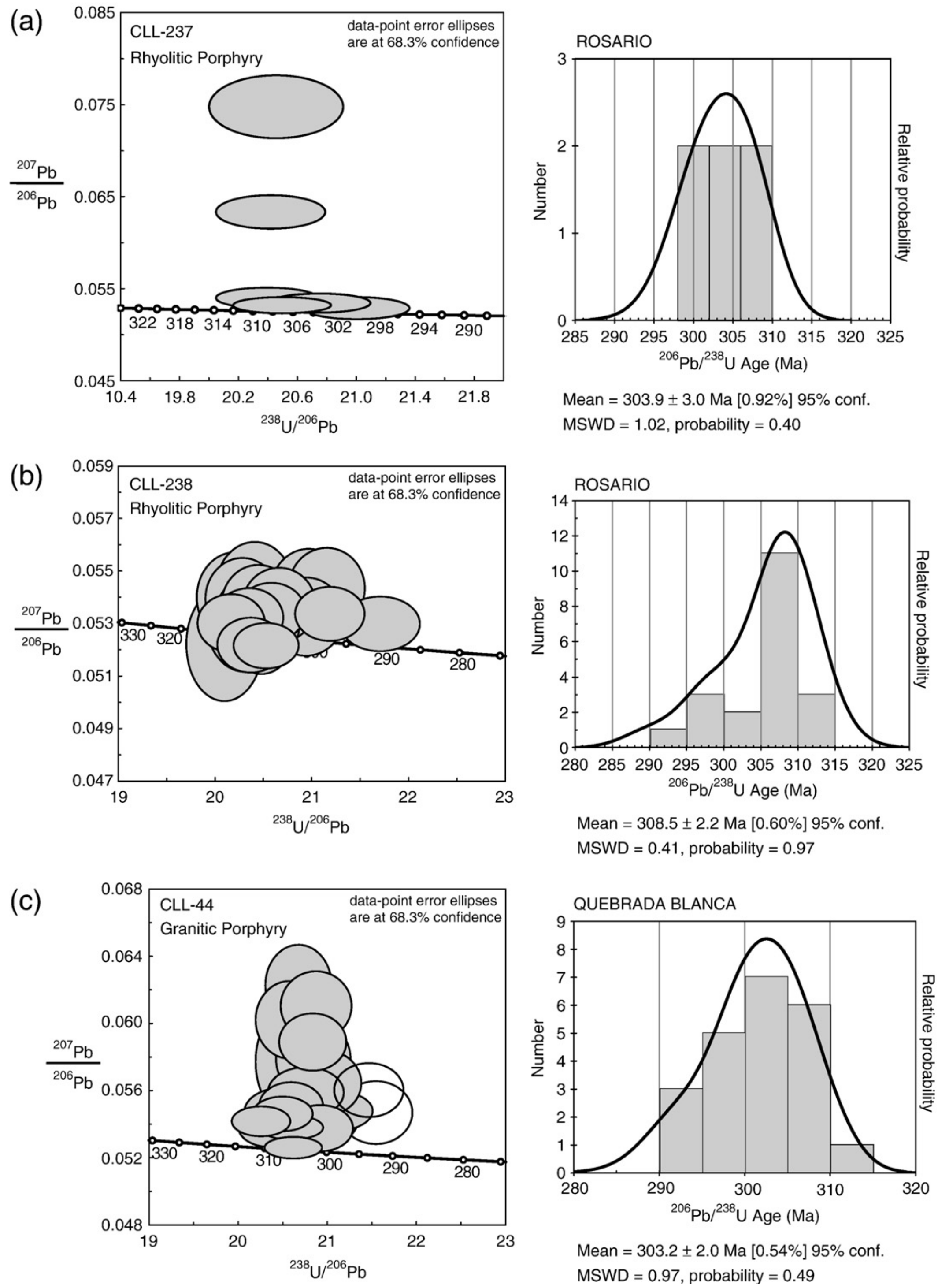

Fig. 4. Tera-Wasserburg concordia plot and probability density plot with stacked histogram of SHRIMP U–Pb age data for: (a) rhyolitic porphyry of Rosario (CLL-237); (b) rhyolitic porphyry of Rosario (CLL-238); and (c) granitic porphyry of Quebrada Blanca (CLL-44).

grouping at about 300 Ma. There is also a younger mode at 244 Ma that is comprised of U–Pb ages for igneous rocks at the La Profunda and Characolla porphyry copper prospects (244.8 ± 2.5 Ma and 243.2 ± 2.1 Ma, respectively, with another Characolla porphyry U–Pb determination giving 248.7 ± 2.4 Ma for three spot analyses; Figs. 6 and 7). The U–Pb ages for these porphyries agree with the laser ICP-MS U–Pb zircon date of 245 ± 12 Ma obtained by Masterman et al. (2004) for the Collahuasi porphyry that is one of the country rocks for the Cenozoic Rosario Cu–Mo porphyry deposit. In addition, we have obtained molybdenite Re–Os ages of 265.5 ± 1.3 and 256.5 ± 1.3 Ma for the Characolla porphyry prospect, but these Re–Os ages are older than the U–Pb age of the Characolla porphyry, probably because of the disturbance of molybdenite

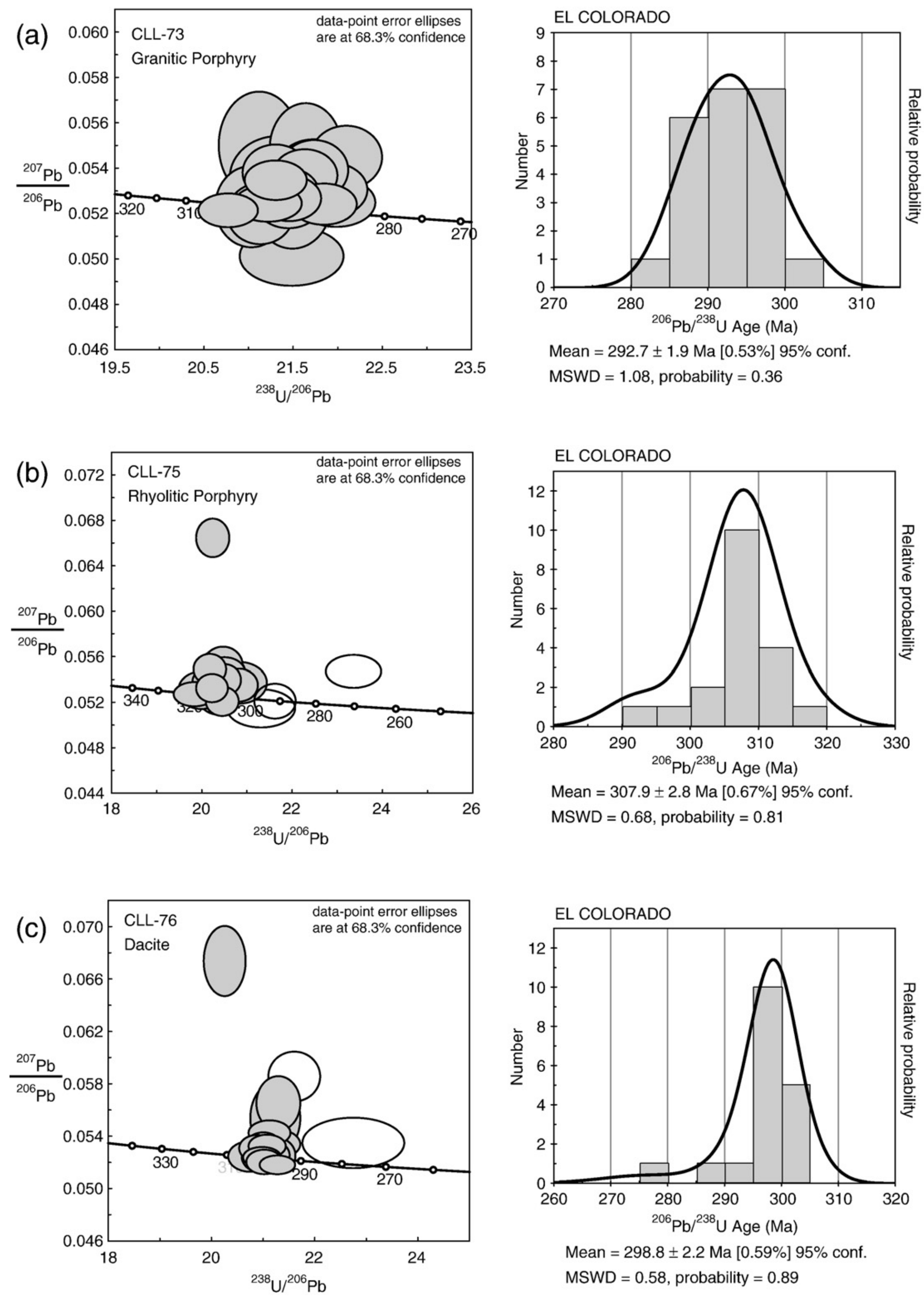

Fig. 5. Tera-Wasserburg concordia plot and probability density plot with stacked histogram of SHRIMP U–Pb age data for: (a) granitic porphyry of El Colorado (CLL-73); (b) rhyolitic porphyry of El Colorado (CLL-75); and (c) dacite (dome) of El Colorado (CLL-76).

Re–Os system (R. Mathur, written commun., 2005). The U–Pb zircon age data substantiate a Triassic porphyry copper mineralization episode that is much older than the larger tonnage and more widely described Cenozoic porphyry copper deposits that are currently mined in the Collahuasi area.

Previous geochronological data for equigranular granitoid plutons for the Andes between 21° and 22°S suggested a time-span of 332 to 245 Ma for magmatism (Table 1; Fig. 1). The new SHRIMP U–Pb zircon ages from 309 to 293 Ma for the oldest population of porphyries and volcanic rocks from the

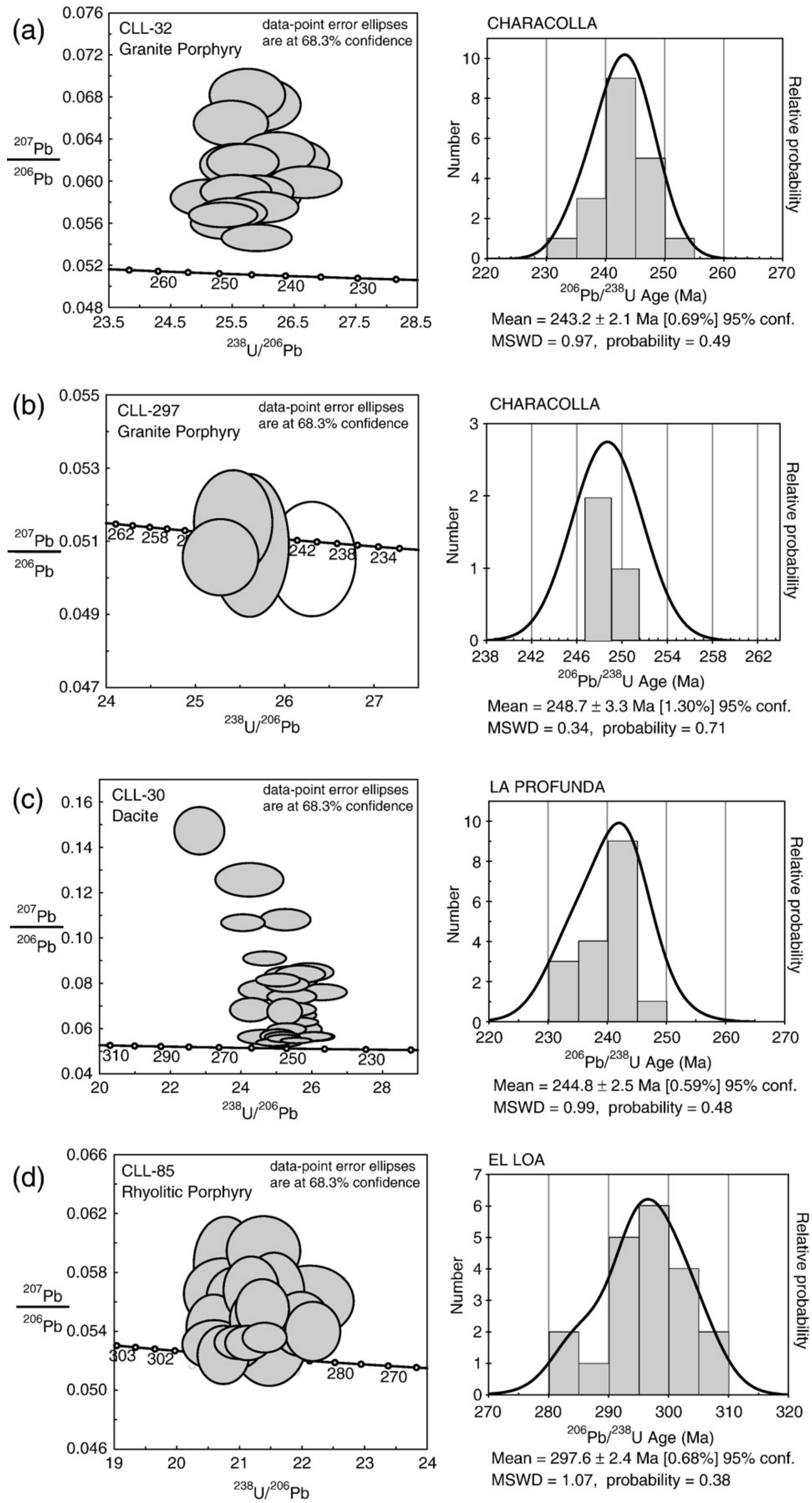

Fig. 6. Tera-Wasserburg concordia plot and probability density plot with stacked histogram of SHRIMP U–Pb age data for: (a) granite porphyry of Characolla (CLL-32); (b) granite porphyry of Characolla (CLL-297); (c) dacite of La Profunda (CLL-30); and (d) rhyolitic porphyry of El Loa (CLL-85).

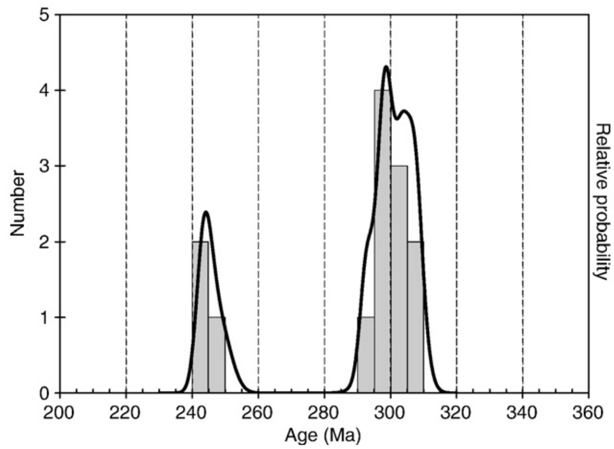

Fig. 7. Probability plot of the SHRIMP zircon U–Pb data. Two peaks are apparent at 300 Ma and 244 Ma, consistent with two discrete magmatic episodes.

Collahuasi Group overlap the previous 293 ± 14 Ma date from the Collahuasi Formation (Masterman, 2003). The new data confirm that there is a temporal relationship between the intrusion of equigranular plutons and the volcanism for the oldest rocks of the Collahuasi Group. It also suggests a discrete ca. 16-m.y.-long period of magmatism in the Late Carboniferous to Early Permian. On the other hand, porphyritic intrusions in the Collahuasi area that are related to porphyry copper mineralization define a second, discrete younger magmatic event at ca. 244 Ma.

6. Petrogenesis

6.1. Introduction

The late Paleozoic–early Mesozoic magmatism from Altos de Pica to Chuquicamata (Fig. 1) is mostly defined by rhyolite and dacite lavas, and granite and granodiorite intrusions; only near Chuquicamata do some relatively small diorite intrusions outcrop. The magmatism in the Collahuasi area began in late Paleozoic with the eruption of a large volume of felsic volcanic rocks, with occasional mafic magmatism, and was considered to be a part of the Choiyoi Magmatic Province defined by Mpodozis and Kay (1990). The volcanism was accompanied by widespread plutonism. The large volume of silicic rocks suggests that this magmatism involved crustal melting (e.g., Lucassen et al., 1999).

Hydrothermal alteration in the Collahuasi area related to Tertiary porphyry copper deposits, particularly silicification and potassic assemblages, has obscured the original chemistry of the rocks and may have impacted the isotopic ratios, particularly for Sr. This is apparent in the chemical data of Masterman (2003) that reports copper contents of even the less altered rocks as being as great as 1.8%. In addition, most of the rocks from the Collahuasi Group fall within the high-K and shoshonitic fields in a SiO_2 versus K_2O diagram, which does not correspond to the igneous composition of what are defined as the least altered rocks (Masterman, 2003).

Widespread late Paleozoic igneous rocks exposed near Calama (Fig. 1) have been interpreted alternatively as the products of arc magmatism (e.g., Brown, 1991; Bahlburg and Hervé, 1997), crustal melts at a passive margin (Breitkreuz and Zeil, 1994, Lucassen et al. 1999, and references therein), or subduction-related, mantle-derived melts with some crustal contamination (Brown, 1991). The latter interpretation assumes a transition from a passive to an active continental margin during Late Carboniferous (Bahlburg, 1993; Bahlburg and Hervé, 1997).

6.2. Sr and Sm–Nd isotopes

Strontium and Nd isotopic data for dacite and rhyodacite from the Collahuasi area are discussed by Masterman, (2003), but due to the intense potassic alteration, the calculated $^{87}Sr/^{86}Sr$ initial ratios (0.6634–0.7024) are mostly not meaningful. Corresponding ε_{Nd} values cluster between −0.53 to +0.13 (recalculated after Masterman, 2003) and are consistent with the involvement of an evolved crustal component. Isotopic data for rocks exposed to the south (near Chuquicamata) have $^{87}Sr/^{86}Sr$ initial ratios from 0.708 to 0.712 and ε_{Nd} from about −2 to −10 (recalculated after Lucassen et al., 1999), which are consistent with a long-lived crustal involvement in the source region for the igneous rocks.

We have measured Sr and Nd isotopes for four new samples of the least altered volcanic rocks from the Collahuasi area; the Sr data are presented in Table 3. Samples from different lithologies and with different textures were selected. The initial $^{87}Sr/^{86}Sr$ ratios, calculated at 300 Ma, cluster at 0.7055–0.7061 (Table 3), excluding sample CLL-293 that yielded a geologically untenable value probably due to unrecognized alteration. The Sm–Nd system appears to have been less affected by the alteration processes and all four samples yield ε_{Nd} values between −1.46 and −1.95 (at 300 Ma, Table 3). These ε_{Nd} values indicate that the rocks have components with some crustal residence time.

6.3. Lu–Hf isotopes

The Hf isotope ratios have been determined for zircon grains from 8 of the 13 samples that were previously dated by SHRIMP U–Pb. It has been demonstrated that zircon is not only of geochronological importance via the U–Th–Pb system, but that the associated Lu–Hf system can be used as a tracer of crustal evolution (e.g., Taylor and McLennan, 1985; Vervoort and Blichert-Toft, 1999; Zhang et al., 2007). Zircons retain their isotopic integrity through multiple episodes of magmatic and sedimentary recycling. More importantly, zircons have very low Lu/Hf ratios (typically ~0.001), so that Hf isotope ratio corrections due to in situ radiogenic growth are virtually negligible. In other words, zircons preserve accurate approximations of the initial $^{176}Hf/^{177}Hf$ ratio of the magma at the time of crystallization (Patchett et al., 1981).

The ε_{Hf} values for the analysed zircons are given in Table 4, with initial Hf values calculated at the U–Pb zircon crystallization age. Initial ε_{Hf} values are mostly positive, being as large as +5.9, but some negative values were obtained for the ca. 300 Ma rocks (Table 4; Fig. 8). For the oldest rocks, two groups

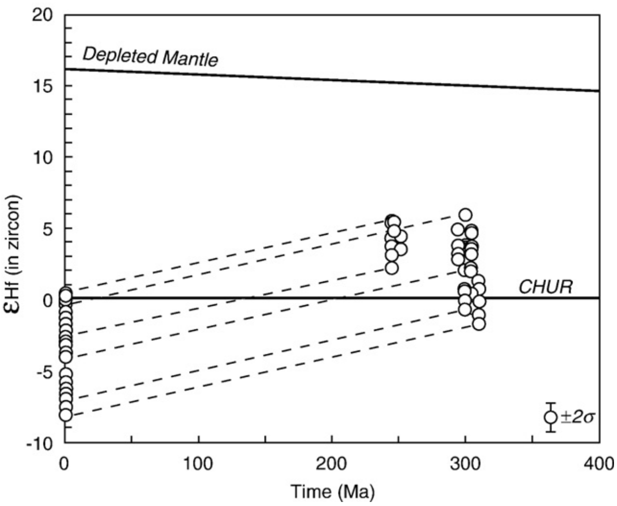

Fig. 8. ε_{Hf}(T) in zircons grains versus the respective SHRIMP U–Pb age; error bar at ±2σ is shown as inset.

are evident: one with ε_{Hf} values from −1.7 to +2.2 (CLL-75; CLL-85; CLL-238); and the other with ε_{Hf} values from about +2.0 to +5.9, with one grain at −0.7 (CLL-44, CLL-73, CLL-76). The 244 Ma rocks show a single cluster with ε_{Hf} values in the range from +2.2 to +5.4 (Fig. 8). The Hf isotope evolution trends are shown on Fig. 8 and indicate that the 300 Ma group with the more evolved signatures could not provide a source for the initial Hf of the 244 Ma magmas. However, the less evolved 300 Ma group could provide the initial Hf at 244 Ma, although it is likely that a small contribution was obtained from a more depleted source (note that the Depleted Mantle ε_{Hf} would be about +15.0 and +15.2 at 300 Ma and 245 Ma, respectively). The overall data indicate that there was a significant contribution of older crustal material to the magmas from which the zircons have crystallized, but also show differences among them giving support to variable magmatic sources or processes for the origin of the rocks of the Collahuasi Group.

7. Discussion and conclusions

Geochronology of the Collahuasi Group has previously been reported based upon poorly-constrained K-feldspar and whole rock K–Ar ages (144 to 39 Ma, recalculated from Huete et al., 1977; Baker, 1977; Vergara and Thomas, 1984; Damm et al., 1986) or limited LA-ICP-MS zircon U–Pb dates of 293 ± 14 Ma for a dacite ignimbrite and 245 ± 12 Ma for a porphyritic granodiorite (Collahuasi porphyry) from the Rosario porphyry copper deposit (Masterman et al., 2005). Tomlinson et al. (2001) first assigned the rocks of the Collahuasi Group to the Late Carboniferous to Early Triassic, based on more regional K–Ar and U–Pb ages of plutonic rocks that were emplaced within the co-genetic volcanic strata between 332 and 245 Ma.

Given the limited and questionable geochronology of igneous rocks in the Collahuasi area, we have carried out SHRIMP U–Pb zircon age determinations. Our new U–Pb data indicate that the Collahuasi Group has two discrete magmatic episodes at ca. 300 Ma and 244 Ma. They also indicate that the Collahuasi Group is the product of temporally discrete magmatic pulses, rather than the result of continuous and widespread magmatism, similarly to the conclusions of Martin et al. (1999) for the equivalent Pastos Blancos Group in the area of the high Andes between 29–30°S.

The slightly negative ε_{Nd} values (−2 to −1.5), together with $^{87}Sr/^{86}Sr$ ratios (0.7056) of volcanic rocks of the Collahuasi Group, are consistent with the involvement of crustal material in the magma genesis. Furthermore, the fact that rocks with different compositions (rhyolite to andesite) show relatively similar ε_{Nd} values Sr initial ratios does not support fractional crystallization or different degrees of melting of a homogeneous parent magma, unless magmatism took place over an unreasonably short time interval.

The range of ε_{Hf} values in zircon from −1.7 to +5.9 suggests that the rocks were derived from different sources or via different processes. The involvement of crustal MORB-type magmas is unlikely, as the rocks derived from such a source would have ε_{Hf} values of about +15. The magma undoubtedly has some component of sedimentary rocks; it probably evolved in the upper crust, most likely in rocks of the metamorphic basement that outcrop near Chuquicamata. In fact, Lucassen et al. (1999) proposed that the late Paleozoic igneous rocks of that region originated during anatexis involving recycling of the basement rocks. Another possible scenario, however, is that the magma composition was a mixture of crustal melts and depleted mantle-derived magmas.

Two clusters of average ε_{Hf} values in zircon at −1.7 to +2.2 and +2.0 to +5.9 for the ca. 300 Ma rocks show a history of different magma sources or processes, with variable degrees of crustal involvement. In addition, average ε_{Hf} values in zircon cluster at about +3.5 to +4.5 for the ca. 244 Ma rocks. This shows that these were derived from relatively less radiogenic source material. This could thus reflect the anatexis of younger rocks or those with less Lu, or involved a mixture between crustal melts and more primitive sub-crustal magma.

The tectonic regime and crustal evolution of this area during late Paleozoic are complex. Llambías and Sato (1995) proposed a cessation of subduction in the Permian and a possible transition from a subduction-related magmatic arc to a collisional regime with crustal thickening, which was followed by Triassic post-orogenic granite magmatism in the Argentinean part of the Cordillera Frontal. Our data are consistent with crustal melting as the main source for the magmatism, but with the addition of Late Carboniferous magmas from other sources, and with Early Triassic contributions from more primitive sources.

Acknowledgements

This study was supported by CONICYT, Chile, through Fondecyt 1030912 grant to F. Munizaga and V. Maksaev (Universidad de Chile). We are grateful to the Doña Inés de Collahuasi and Quebrada Blanca mining companies that granted access for sampling at their mines, prospects, and drillcores, and supplied geological information. We are particularly thankful to Ricardo Palma, Manuel Durán, and Jean Philippe Desrochers. The geologists Claudio Bisso, Claudio Ahumada, Leonardo Torres, Sergio Giglio, Patricio Osorio, Jorge Zamorano, Boris Alarcón, Pedro Apablaza, Michael Buchanan, Marcial Vergara, and Alejandro Sanhueza greatly facilitated our work at the high altitude of Collahuasi. Helpful comments by Suzanne M. Kay, David Chew and Richard Goldfarb are greatly appreciated.

Appendix A. Analytical procedures

A.1. U–Pb SHRIMP

Zircon grains were obtained from samples of the Collahuasi Group and associated intrusive rocks following normal mineral separation procedures, which included crushing, washing, and heavy liquid and magnetic separation. Hand-picked zircon grains were mounted in epoxy, together with chips of the FC1 or Temora reference zircons, sectioned approximately in one-half, and polished. Reflected and transmitted light photomicrographs were prepared for all zircons, as were cathodoluminescence (CL) Scanning Electron Microscope (SEM) images. The CL images were used to decipher the internal structures of the sectioned grains and to ensure that the ~20 μm SHRIMP spot was wholly within a single age component within the sectioned grains. Uranium–Th–Pb analyses were made using a sensitive high resolution ion microprobe (SHRIMP II) for determining the respective zircon $^{238}U/^{206}Pb$ ages following procedures given in Williams (1998, and references therein). Analytic work was done at the Research School of Earth Sciences, The Australian National University, Canberra, Australia. Each analysis consisted of six scans through the mass range, with a FC1 or Temora U–Pb reference grain analyzed for every three unknown analyses. The data have been reduced using the SQUID Excel Macro of Ludwig (2001); U/Pb ratios have been normalized relative to a value of 0.0668 for the Temora reference zircon, equivalent to an age of 417 Ma (see Black et al., 2003). Uncertainties given for individual analyses (ratios and ages) are at the one-sigma level (see Appendix A). Tera and Wasserburg (1972) concordia plots, probability density plots with stacked histograms, and weighted mean $^{206}Pb/^{238}U$ age calculations were carried out using ISOPLOT/EX (Ludwig, 2003). Weighted mean $^{206}Pb/^{238}U$ ages have been calculated and the uncertainties are reported as 95% confidence limits.

A.2. Hf isotopes

The measurements were conducted by laser ablation multi-collector inductively coupled plasma mass spectroscopy using a RSES Neptune MC-ICPMS coupled with a HelEx 193 μm ArF Excimer laser ablation system (Eggins, 2003; Eggins et al., 2005). Samples were photographed under a reflected light microscope subsequent to U–Pb dating by SHRIMP to reveal the location on each grain of the ion probe sputter pit (typically about 20 μm across). Laser ablation analyses were performed on the same locations. For most analyses of unknowns or secondary standards, the laser spot size on the sample was either 47 or 37 μm in diameter, depending on the size of the grain and the nature of internal structure as revealed by CL imaging. The mass spectrometer was first tuned to optimal sensitivity using a large grain of zircon from the Monastery kimberlite.

The detector array was as follows:

Cup	L4	L3	L2	L1	C	H1	H2	H3	H4
Mass	171	173	174	175	176	177	178	179	181

All listed masses were measured simultaneously in static-collection mode. A gas blank was acquired at regular intervals throughout the analytical session (every ten analyses).

The laser was pulsed with a repetition rate of 5–8 Hz and applied fluence of ~5 J/m^2 at the target site. Data were acquired for 100 s, but in many cases only a selected interval from the total acquisition was used in data reduction. In each batch of samples between gas blank measurements, several secondary standard zircons (91500, FC-1, Temora-2, Monastery and Mud Tank) were measured to assess data quality.

Measured signal intensity was typically ≈ 5–6 V total Hf at the beginning of ablation, and decreased over the acquisition period to 2 V or less. Isobaric interferences of ^{176}Lu and ^{176}Yb on the ^{176}Hf signal were corrected by monitoring signal intensities of ^{175}Lu and ^{173}Yb and ^{171}Yb. The interference of ^{174}Yb on ^{174}Lu was also corrected from the monitored ^{173}Yb and ^{171}Yb isotopes. These Lu and Yb isobar interferences were corrected using an exponential mass fractionation beta coefficient based on reference of the measured $^{173}Yb/^{171}Yb$ to the atomic ratio of 1.123456 proposed by Thirwall and Anczkiewicz (2004), and the Yb and Lu isotope ratio compositions reported by Thirwall and Anczkiewicz (2004), and Chu et al. (2002), respectively. In cases where zircon Yb contents were too low to measure $^{173}Yb/^{171}Yb$ to an internal precision better than 4%, the applied Yb and Lu beta coefficient was estimated from the measured Hf beta coefficient, based on the measured in-run ratio of the Yb and Hf beta coefficients. The latter was found typically to have a value near 1.30, consistent with the relationship reported by Chu et al. (2002). Interference corrected Hf isotopes ratios were subsequently corrected for instrumental mass fractionation using an exponential law based on reference of the measured $^{179}Hf/^{177}Hf$ to the atomic ratio of 0.7325 proposed by Thirwall and Anczkiewicz (2004). The determined $^{174}Hf/^{177}Hf$ ratio used to assess the veracity of the correction procedure applied to Lu and Yb isotope interferences on ^{174}Hf and ^{176}Hf.

A.3. Sr and Sm–Nd isotopes

The Rb–Sr and Sm–Nd isotopic analysis were carried out at Geochronological Research Center of the University of Sao Paulo, Brazil. The samples for analysis were prepared by standard methods according to the analytical procedures described by Tassinari et al. (1996), involving HF-HNO_3

dissolution and HCl cation exchange. No visible solid residues were observed after dissolution. Samples with incomplete dissolution were discarded. The Sr isotopic ratios were normalized to $^{86}Sr/^{88}Sr = 0.1194$; replicate analyses of $^{87}Sr/^{86}Sr$ for the NBS987 standard gave a mean value of 0.71028 ± 0.00006 (2σ), the blanks for Sr were 5 ng. Nd ratios were normalized to a 146Nd/144Nd = 0.72190. The averages of 143Nd/^{144}Nd for La Jolla and BCR-1 standards were 0.511847 ± 0.00005 (2σ) and 0.512662 ± 0.00005 (2σ), respectively. The blanks were less than 0.03 ng. The Sr and Nd isotope analyses were carried out on a multi-collector Finnigan-MAT 262 mass spectrometer. The isotopic data were regressed using the decay constants established in Steiger and Jaeger (1977); for $^{87}Rb = 1.42 \times 10^{-11}$ yr^{-1}; for 147Sm = 6.54×10^{-12} yr^{-1}.

Appendix B. Zircon SHRIMP U–Pb analytical data for rocks of the Collahuasi Group

							Total				Radiogenic		Age (Ma)	
Grain. spot	U (ppm)	Th (ppm)	Th/U	$^{206}Pb^*$ (ppm)	$^{204}Pb/^{206}Pb$	f_{206} %	$^{238}U/^{206}Pb$	±	$^{207}Pb/^{206}Pb$	±	$^{206}Pb/^{238}U$	±	$^{206}Pb/^{238}U$	±
Sample CLL-44														
1.1	170	76	0.45	6.8	0.000494	0.48	21.47	0.26	0.0560	0.0011	0.0464	0.0006	292.1	3.5
2.1	371	77	0.21	15.5	0.000262	0.26	20.50	0.22	0.0546	0.0007	0.0487	0.0005	306.2	3.3
3.1	469	78	0.17	19.8	0.000038	0.16	20.36	0.23	0.0538	0.0008	0.0490	0.0006	308.7	3.5
4.1	123	79	0.64	4.9	0.000109	0.31	21.55	0.27	0.0547	0.0012	0.0463	0.0006	291.5	3.6
5.1	969	76	0.08	40.4	0.000077	0.01	20.62	0.21	0.0526	0.0004	0.0485	0.0005	305.2	3.1
5.2	89	71	0.80	3.7	0.000223	0.69	20.85	0.28	0.0578	0.0015	0.0476	0.0006	300.0	4.0
6.1	157	75	0.48	6.5	0.000797	0.81	20.84	0.25	0.0589	0.0011	0.0476	0.0006	299.8	3.6
7.1	142	79	0.55	5.8	–	0.33	20.99	0.26	0.0549	0.0015	0.0475	0.0006	299.0	3.6
8.1	115	76	0.66	4.7	0.000607	1.08	20.88	0.27	0.0610	0.0014	0.0474	0.0006	298.4	3.8
9.1	220	74	0.34	9.0	0.000132	0.17	20.93	0.24	0.0537	0.0009	0.0477	0.0006	300.4	3.4
10.1	272	77	0.28	11.1	0.000149	0.31	21.03	0.32	0.0548	0.0008	0.0474	0.0007	298.6	4.5
11.1	184	76	0.42	7.6	0.000370	0.43	20.76	0.28	0.0559	0.0010	0.0480	0.0007	302.0	4.1
12.1	105	73	0.69	4.4	0.000212	0.66	20.60	0.27	0.0577	0.0022	0.0482	0.0007	303.6	4.0
13.1	205	74	0.36	8.6	0.000604	0.32	20.59	0.24	0.0550	0.0010	0.0484	0.0006	304.7	3.5
14.1	773	78	0.10	32.2	0.000082	0.16	20.60	0.24	0.0538	0.0005	0.0485	0.0006	305.1	3.5
15.1	119	75	0.63	4.9	0.000431	0.51	20.99	0.26	0.0564	0.0013	0.0474	0.0006	298.6	3.7
16.1	510	72	0.14	21.6	0.000068	0.20	20.26	0.22	0.0541	0.0006	0.0493	0.0005	310.0	3.3
17.1	133	76	0.57	5.6	0.000372	0.97	20.58	0.25	0.0602	0.0015	0.0481	0.0006	303.0	3.7
18.1	170	78	0.46	7.1	0.000198	1.23	20.68	0.25	0.0622	0.0016	0.0478	0.0006	300.8	3.6
18.2	192	74	0.39	20.3	0.000141	0.15	8.110	0.098	0.0654	0.0007	0.1231	0.0015	748.5	8.7
19.1	194	76	0.39	8.1	0.000007	0.28	20.52	0.30	0.0547	0.0010	0.0486	0.0007	305.9	4.4
20.1	140	79	0.56	5.9	0.003423	5.69	20.40	0.25	0.0978	0.0070	0.0462	0.0008	291.4	4.9
21.1	108	78	0.72	4.5	0.000557	0.66	20.50	0.26	0.0577	0.0013	0.0485	0.0006	305.0	3.9
							Weighted mean $^{206}Pb/^{238}U$ age 292.7 ± 2.0 Ma							
Sample CLL-73														
1.1	576	903	1.57	22.6	0.000022	0.04	21.843	0.244	0.0524	0.0006	0.0458	0.0005	288.5	3.2
2.1	266	343	1.29	10.5	0.000236	0.21	21.788	0.301	0.0538	0.0009	0.0458	0.0006	288.7	3.9
3.1	263	401	1.52	10.5	–	<0.01	21.483	0.384	0.0501	0.0009	0.0467	0.0008	294.0	5.2
4.1	179	174	0.98	7.1	–	0.34	21.638	0.267	0.0548	0.0013	0.0461	0.0006	290.3	3.6
5.1	265	366	1.38	10.3	0.000010	0.31	22.097	0.265	0.0544	0.0009	0.0451	0.0005	284.5	3.4
6.1	452	416	0.92	18.1	0.000041	0.09	21.419	0.236	0.0529	0.0007	0.0466	0.0005	293.9	3.2
7.1	286	407	1.42	11.3	0.000257	0.23	21.730	0.275	0.0539	0.0009	0.0459	0.0006	289.4	3.6
8.1	418	585	1.40	16.8	0.000065	0.03	21.447	0.239	0.0524	0.0007	0.0466	0.0005	293.7	3.2
9.1	287	47	0.16	11.3	0.000028	0.23	21.732	0.251	0.0539	0.0009	0.0459	0.0005	289.4	3.3
10.1	423	613	1.45	16.5	0.000149	0.06	21.984	0.290	0.0525	0.0007	0.0455	0.0006	286.6	3.7
11.1	386	353	0.91	15.3	0.000037	0.19	21.627	0.243	0.0536	0.0008	0.0462	0.0005	290.9	3.2
12.1	362	322	0.89	14.2	–	0.12	21.916	0.275	0.0530	0.0008	0.0456	0.0006	287.3	3.6
13.1	499	987	1.98	20.0	0.000025	0.06	21.456	0.236	0.0527	0.0007	0.0466	0.0005	293.5	3.2
14.1	119	123	1.04	4.8	0.000204	0.04	21.491	0.292	0.0525	0.0014	0.0465	0.0006	293.1	4.0
15.1	158	168	1.06	6.4	0.000114	0.17	21.315	0.354	0.0536	0.0012	0.0468	0.0008	295.1	4.9
16.1	742	888	1.20	29.9	–	0.15	21.303	0.228	0.0535	0.0006	0.0469	0.0005	295.3	3.1
17.1	162	152	0.93	6.6	0.000571	<0.01	21.030	0.268	0.0523	0.0012	0.0476	0.0006	299.5	3.8
18.1	284	383	1.35	11.5	0.000248	<0.01	21.128	0.247	0.0520	0.0009	0.0473	0.0006	298.2	3.5
19.1	101	108	1.06	4.1	0.000756	0.34	21.116	0.301	0.0550	0.0016	0.0472	0.0007	297.3	4.2
20.1	793	1403	1.77	32.1	0.000071	0.02	21.219	0.249	0.0524	0.0005	0.0471	0.0006	296.8	3.4
21.1	360	503	1.40	14.5	0.000138	0.19	21.302	0.244	0.0538	0.0008	0.0469	0.0005	295.2	3.3
22.1	947	1326	1.40	39.2	0.000060	<0.01	20.769	0.220	0.0521	0.0005	0.0482	0.0005	303.3	3.2
							Weighted mean $^{206}Pb/^{238}U$ age 292.7 ± 1.9 Ma							

(continued on next page)

Appendix B (*continued*)

Grain. spot	U (ppm)	Th (ppm)	Th/U	$^{206}Pb^*$ (ppm)	$^{204}Pb/^{206}Pb$	f_{206} %	Total $^{238}U/^{206}Pb$	±	$^{207}Pb/^{206}Pb$	±	Radiogenic $^{206}Pb/^{238}U$	±	Age (Ma) $^{206}Pb/^{238}U$	±
Sample CLL-114														
1.1	152	69	0.45	6.4	0.000408	0.17	20.36	0.25	0.0539	0.0011	0.0490	0.0006	308.6	3.8
2.1	106	53	0.50	4.3	–	0.19	21.03	0.28	0.0538	0.0013	0.0475	0.0006	299.0	3.9
3.1	188	94	0.50	7.8	0.000333	<0.01	20.66	0.25	0.0522	0.0009	0.0484	0.0006	304.8	3.6
4.1	626	113	0.18	19.6	0.000148	0.23	27.46	0.29	0.0526	0.0006	0.0363	0.0004	230.1	2.4
5.1	320	156	0.49	13.4	0.000029	0.15	20.51	0.28	0.0537	0.0008	0.0487	0.0007	306.4	4.1
6.1	345	204	0.59	14.4	0.000005	0.10	20.61	0.23	0.0533	0.0007	0.0485	0.0005	305.1	3.4
7.1	166	109	0.66	6.8	0.000242	<0.01	20.79	0.30	0.0514	0.0010	0.0482	0.0007	303.3	4.3
							Weighted mean $^{206}Pb/^{238}U$ age 304.6 ± 3.2 Ma							
Sample CLL-76														
1.1	491	393	0.80	20.2	0.000091	0.09	20.882	0.230	0.0531	0.0007	0.0478	0.0005	301.3	3.3
2.1	69	32	0.46	2.8	0.000465	0.39	21.241	0.323	0.0553	0.0018	0.0469	0.0007	295.4	4.5
3.1	345	323	0.94	14.0	0.000174	0.14	21.194	0.353	0.0534	0.0008	0.0471	0.0008	296.8	4.9
4.1	656	903	1.38	26.7	0.000100	0.11	21.084	0.239	0.0532	0.0006	0.0474	0.0005	298.4	3.3
5.1	139	91	0.66	5.2	0.000113	0.21	22.758	0.655	0.0534	0.0013	0.0439	0.0013	276.7	7.9
6.1	588	524	0.89	23.9	–	0.24	21.131	0.271	0.0542	0.0006	0.0472	0.0006	297.4	3.8
7.1	571	517	0.90	23.3	–	<0.01	21.027	0.229	0.0520	0.0006	0.0476	0.0005	299.6	3.2
8.1	842	946	1.12	34.5	–	<0.01	20.984	0.245	0.0524	0.0005	0.0477	0.0006	300.1	3.5
9.1	134	71	0.53	5.4	0.000544	0.53	21.303	0.283	0.0565	0.0014	0.0467	0.0006	294.2	3.9
10.1	1032	1851	1.79	41.7	0.000037	<0.01	21.290	0.227	0.0518	0.0005	0.0470	0.0005	296.1	3.1
11.1	283	185	0.65	11.4	0.000067	0.03	21.251	0.255	0.0525	0.0009	0.0470	0.0006	296.3	3.5
12.1	427	200	0.47	17.3	–	0.03	21.166	0.237	0.0525	0.0007	0.0472	0.0005	297.5	3.3
13.1	444	548	1.23	18.0	–	<0.01	21.177	0.302	0.0522	0.0007	0.0472	0.0007	297.5	4.2
14.1	344	197	0.57	14.2	–	<0.01	20.751	0.279	0.0524	0.0008	0.0482	0.0007	303.4	4.0
15.1	656	688	1.05	26.9	0.000065	0.01	20.919	0.225	0.0525	0.0008	0.0478	0.0005	301.0	3.2
16.1	454	458	1.01	18.6	0.000052	0.11	21.008	0.231	0.0532	0.0007	0.0475	0.0005	299.4	3.3
17.1	119	54	0.45	5.0	0.000585	1.85	20.257	0.269	0.0673	0.0018	0.0485	0.0007	305.0	4.1
18.1	154	56	0.36	6.1	0.000029	0.80	21.609	0.334	0.0585	0.0012	0.0459	0.0007	289.3	4.4
							Weighted mean $^{206}Pb/^{238}U$ age 298.8 ± 2.2 Ma							
Sample CLL-85														
1.1	169	123	0.73	7.0	–	0.18	20.934	0.334	0.0538	0.0016	0.0477	0.0008	300.3	4.8
2.1	189	106	0.56	7.9	0.000305	0.08	20.595	0.337	0.0531	0.0011	0.0485	0.0008	305.4	4.9
3.1	102	81	0.79	4.0	0.000326	0.51	22.134	0.465	0.0560	0.0016	0.0449	0.0010	283.4	5.9
4.1	57	38	0.68	2.3	0.000975	0.77	20.785	0.339	0.0586	0.0021	0.0477	0.0008	300.6	4.9
5.1	97	51	0.53	4.1	–	0.21	20.583	0.290	0.0542	0.0015	0.0485	0.0007	305.2	4.3
6.1	135	73	0.54	5.5	0.000389	0.25	21.174	0.384	0.0543	0.0013	0.0471	0.0009	296.8	5.3
7.1	381	190	0.50	15.5	–	0.11	21.133	0.238	0.0532	0.0008	0.0473	0.0005	297.7	3.3
8.1	59	49	0.83	2.4	0.000487	0.14	21.479	0.393	0.0533	0.0020	0.0465	0.0009	293.0	5.3
9.1	104	80	0.77	4.2	0.000551	0.57	21.190	0.293	0.0568	0.0015	0.0469	0.0007	295.6	4.1
10.1	93	40	0.43	3.9	0.000741	0.51	20.726	0.408	0.0565	0.0016	0.0480	0.0010	302.2	5.9
11.1	123	113	0.92	5.0	–	0.49	20.992	0.340	0.0563	0.0014	0.0474	0.0008	298.6	4.8
12.1	380	163	0.43	15.5	0.000002	0.11	20.989	0.254	0.0532	0.0007	0.0476	0.0006	299.7	3.6
13.1	113	76	0.68	4.4	0.000002	0.31	21.989	0.313	0.0545	0.0014	0.0453	0.0007	285.8	4.0
14.1	130	71	0.54	5.2	0.000103	0.41	21.369	0.282	0.0555	0.0013	0.0466	0.0006	293.6	3.8
15.1	127	85	0.67	5.2	0.000035	<0.01	20.746	0.274	0.0524	0.0013	0.0482	0.0006	303.5	4.0
16.1	104	88	0.84	4.2	0.000462	0.91	21.387	0.391	0.0594	0.0016	0.0463	0.0009	292.0	5.3
17.1	517	258	0.50	20.7	0.000149	0.17	21.407	0.234	0.0535	0.0007	0.0466	0.0005	293.8	3.2
18.1	121	80	0.66	4.9	0.000635	0.31	21.278	0.284	0.0547	0.0014	0.0469	0.0006	295.2	3.9
19.1	81	64	0.79	3.2	0.000883	0.56	21.555	0.321	0.0566	0.0018	0.0461	0.0007	290.7	4.3
20.1	132	128	0.96	5.1	0.000087	0.25	22.179	0.291	0.0539	0.0013	0.0450	0.0006	283.6	3.7
							Weighted mean $^{206}Pb/^{238}U$ age 297.6 ± 2.4 Ma							
Sample CLL-75														
1.1	290	170	0.58	12.2	–	0.25	20.501	0.305	0.0545	0.0009	0.0487	0.0007	306.3	4.5
2.1	246	166	0.67	10.2	0.000057	0.14	20.819	0.277	0.0535	0.0010	0.0480	0.0006	302.0	4.0
3.1	145	82	0.57	6.1	0.000064	0.03	20.363	0.317	0.0528	0.0013	0.0491	0.0008	309.0	4.8
4.1	293	138	0.47	12.3	0.000147	0.18	20.503	0.240	0.0539	0.0009	0.0487	0.0006	306.5	3.6
5.1	192	105	0.55	8.3	0.000070	0.04	19.986	0.333	0.0530	0.0011	0.0500	0.0008	314.6	5.2
6.1	361	177	0.49	15.3	0.000034	0.08	20.226	0.232	0.0532	0.0008	0.0494	0.0006	310.9	3.5
7.1	99	39	0.40	4.2	0.000752	0.18	20.280	0.295	0.0540	0.0016	0.0492	0.0007	309.7	4.5

Appendix B (*continued*)

							Total				Radiogenic		Age (Ma)	
Grain. spot	U (ppm)	Th (ppm)	Th/U	$^{206}Pb^{*}$ (ppm)	$^{204}Pb/^{206}Pb$	f_{206} %	$^{238}U/^{206}Pb$	±	$^{207}Pb/^{206}Pb$	±	$^{206}Pb/^{238}U$	±	$^{206}Pb/^{238}U$	±
Sample CLL-75														
8.1	194	116	0.60	7.8	0.000294	<0.01	21.321	0.498	0.0514	0.0011	0.0469	0.0011	295.8	6.8
9.1	345	177	0.51	14.5	0.000041	<0.01	20.453	0.239	0.0520	0.0009	0.0489	0.0006	307.9	3.6
10.1	257	148	0.57	10.2	–	<0.01	21.627	0.308	0.0521	0.0010	0.0462	0.0007	291.4	4.1
11.1	366	199	0.54	15.3	0.000028	0.05	20.496	0.305	0.0529	0.0008	0.0488	0.0007	306.9	4.5
12.1	97	35	0.36	4.0	0.000109	0.18	20.565	0.285	0.0539	0.0015	0.0485	0.0007	305.5	4.2
13.1	139	47	0.34	5.7	0.000140	0.16	20.835	0.403	0.0537	0.0012	0.0479	0.0009	301.7	5.8
14.1	284	158	0.56	12.1	–	0.28	20.180	0.239	0.0549	0.0009	0.0494	0.0006	310.9	3.6
15.1	135	77	0.57	5.7	0.000503	0.17	20.438	0.425	0.0538	0.0013	0.0488	0.0010	307.4	6.3
16.1	468	281	0.60	20.3	0.000077	<0.01	19.840	0.304	0.0527	0.0007	0.0504	0.0008	317.0	4.8
17.1	308	159	0.52	13.1	0.000053	0.14	20.207	0.275	0.0537	0.0009	0.0494	0.0007	310.9	4.2
18.1	272	158	0.58	10.0	0.000175	0.38	23.373	0.409	0.0547	0.0010	0.0426	0.0008	269.1	4.7
19.1	201	118	0.59	8.4	0.000006	0.34	20.470	0.287	0.0552	0.0011	0.0487	0.0007	306.5	4.3
20.1	203	131	0.64	8.6	0.001439	1.73	20.238	0.244	0.0664	0.0011	0.0486	0.0006	305.7	3.7
							Weighted mean $^{206}Pb/^{238}U$ age 307.9 ± 2.8 Ma							
Sample CLL-221														
1.1	269	108	0.40	10.5	0.000384	0.54	22.04	0.43	0.0563	0.0011	0.0451	0.0009	284.5	5.5
2.1	319	201	0.63	12.6	0.000181	0.34	21.74	0.35	0.0548	0.0010	0.0458	0.0007	288.9	4.5
3.1	299	201	0.67	12.0	0.000219	0.49	21.35	0.51	0.0561	0.0010	0.0466	0.0011	293.7	6.9
4.1	322	184	0.57	12.9	0.000147	0.21	21.42	0.26	0.0539	0.0010	0.0466	0.0006	293.6	3.6
5.1	271	137	0.51	11.2	–	<0.01	20.80	0.26	0.0515	0.0012	0.0481	0.0006	303.0	3.8
6.1	281	189	0.67	11.4	0.000248	0.08	21.20	0.27	0.0529	0.0010	0.0471	0.0006	296.9	3.7
7.1	379	278	0.73	15.4	0.000142	<0.01	21.14	0.25	0.0521	0.0009	0.0473	0.0006	298.0	3.5
8.1	394	240	0.61	16.3	0.000139	0.05	20.76	0.25	0.0528	0.0009	0.0482	0.0006	303.2	3.6
9.1	294	158	0.54	12.8	0.000000	0.55	19.69	0.38	0.0572	0.0013	0.0505	0.0010	317.6	6.0
10.1	342	210	0.61	14.3	0.000148	0.16	20.59	0.25	0.0538	0.0009	0.0485	0.0006	305.2	3.6
10.2	157	69	0.44	6.3	0.000631	0.18	21.51	0.30	0.0536	0.0014	0.0464	0.0007	292.3	4.1
							Weighted Mean $^{206}Pb/^{238}U$ Age 296.9 ± 4.6 Ma							
Sample CLL-223														
1.1	357	193	0.54	13.3	0.000358	0.19	23.00	0.28	0.0533	0.0011	0.0434	0.0005	273.9	3.3
2.1	261	157	0.60	10.3	–	0.16	21.83	0.28	0.0534	0.0020	0.0457	0.0006	288.3	3.7
3.1	137	97	0.71	5.5	0.000099	0.34	21.49	0.32	0.0549	0.0016	0.0464	0.0007	292.3	4.3
4.1	313	189	0.60	13.0	0.000194	0.01	20.76	0.26	0.0525	0.0010	0.0482	0.0006	303.3	3.7
5.1	242	132	0.55	9.9	0.000167	0.19	21.07	0.27	0.0538	0.0012	0.0474	0.0006	298.3	3.8
6.1	387	245	0.63	15.9	–	0.20	20.86	0.25	0.0540	0.0012	0.0479	0.0006	301.3	3.6
7.1	378	244	0.65	15.6	–	0.04	20.84	0.25	0.0527	0.0009	0.0480	0.0006	302.1	3.5
8.1	112	82	0.73	4.5	–	0.06	21.45	0.33	0.0527	0.0016	0.0466	0.0007	293.6	4.5
9.1	201	136	0.68	8.2	0.000390	0.28	20.95	0.28	0.0546	0.0015	0.0476	0.0006	299.7	4.0
10.1	241	204	0.84	10.2	0.000390	<0.01	20.32	0.26	0.0522	0.0011	0.0492	0.0006	309.8	3.9
11.1	299	168	0.56	12.2	0.000263	0.44	21.13	0.26	0.0558	0.0010	0.0471	0.0006	296.8	3.6
12.1	110	69	0.63	4.4	0.000296	0.35	21.28	0.33	0.0550	0.0017	0.0468	0.0007	295.0	4.5
13.1	208	153	0.74	8.6	0.000300	<0.01	20.71	0.27	0.0513	0.0012	0.0483	0.0006	304.3	4.0
15.1	317	280	0.89	12.8	0.000147	0.20	21.17	0.26	0.0538	0.0010	0.0472	0.0006	297.0	3.6
16.1	306	179	0.58	12.3	0.000364	0.17	21.37	0.27	0.0536	0.0010	0.0467	0.0006	294.3	3.6
17.1	118	84	0.71	4.7	–	0.23	21.51	0.33	0.0540	0.0017	0.0464	0.0007	292.3	4.5
18.1	312	173	0.56	12.7	0.000332	0.17	21.00	0.26	0.0537	0.0010	0.0475	0.0006	299.4	3.7
19.1	154	101	0.66	6.2	0.000676	<0.01	21.17	0.30	0.0516	0.0014	0.0473	0.0007	297.8	4.2
20.1	240	97	0.40	9.8	0.000270	<0.01	20.96	0.31	0.0523	0.0012	0.0477	0.0007	300.5	4.4
							Weighted Mean $^{206}Pb/^{238}U$ Age 298.3 ± 2.1 Ma							
CLL-237														
1.1	172	99	0.57	7.3	0.000817	1.36	20.41	0.25	0.0634	0.0012	0.0483	0.0006	304.2	3.6
2.1	63	26	0.41	2.7	0.001638	2.80	20.45	0.30	0.0748	0.0023	0.0475	0.0007	299.4	4.4
3.1	310	175	0.56	13.1	–	0.19	20.38	0.23	0.0540	0.0007	0.0490	0.0006	308.2	3.4
4.1	638	412	0.65	26.7	0.000082	0.10	20.49	0.22	0.0533	0.0006	0.0488	0.0005	306.9	3.3
5.1	343	185	0.54	14.0	0.000093	0.08	21.00	0.24	0.0529	0.0008	0.0476	0.0005	299.7	3.4
6.1	442	200	0.45	18.3	0.000204	0.14	20.75	0.23	0.0535	0.0007	0.0481	0.0005	303.1	3.3
							Weighted Mean $^{206}Pb/^{238}U$ Age 303.9 ± 3.0 Ma							

(continued on next page)

Appendix B (*continued*)

Grain. spot	U (ppm)	Th (ppm)	Th/U	^{206}Pb* (ppm)	^{204}Pb/^{206}Pb	f_{206} %	Total ^{238}U/^{206}Pb	±	^{207}Pb/^{206}Pb	±	Radiogenic ^{206}Pb/^{238}U	±	Age (Ma) ^{206}Pb/^{238}U	±
Sample CLL-238														
1.1	356	201	0.56	14.9	–	0.12	20.57	0.23	0.0534	0.0007	0.0485	0.0006	305.6	3.4
2.1	389	217	0.56	16.4	–	<0.01	20.36	0.23	0.0521	0.0007	0.0491	0.0006	309.2	3.4
3.1	451	237	0.53	17.9	0.000319	0.11	21.70	0.27	0.0530	0.0007	0.0460	0.0006	290.1	3.6
4.1	368	195	0.53	15.5	0.000232	0.08	20.34	0.23	0.0532	0.0007	0.0491	0.0006	309.1	3.5
5.1	201	107	0.53	8.5	0.000333	0.15	20.44	0.25	0.0537	0.0010	0.0488	0.0006	307.4	3.7
6.1	361	217	0.60	15.4	0.000142	0.05	20.16	0.23	0.0530	0.0007	0.0496	0.0006	311.9	3.5
7.1	178	108	0.61	7.5	0.000826	0.09	20.47	0.26	0.0532	0.0014	0.0488	0.0006	307.2	3.9
8.1	155	77	0.49	6.6	–	0.17	20.20	0.26	0.0540	0.0011	0.0494	0.0006	311.0	4.0
9.1	438	241	0.55	17.8	0.000099	0.13	21.18	0.24	0.0533	0.0007	0.0471	0.0005	297.0	3.3
10.1	152	101	0.66	6.4	–	0.04	20.31	0.26	0.0529	0.0011	0.0492	0.0006	309.7	4.0
11.1	604	391	0.65	25.3	–	<0.01	20.52	0.22	0.0521	0.0006	0.0487	0.0005	306.8	3.3
12.1	163	90	0.55	6.9	–	0.23	20.41	0.26	0.0544	0.0011	0.0489	0.0006	307.7	3.9
13.1	184	85	0.46	7.6	0.000204	0.23	20.96	0.26	0.0542	0.0011	0.0476	0.0006	299.7	3.7
14.1	229	137	0.60	9.6	0.000008	0.05	20.49	0.25	0.0529	0.0009	0.0488	0.0006	307.0	3.7
15.1	216	132	0.61	8.9	0.000429	0.11	20.93	0.26	0.0532	0.0010	0.0477	0.0006	300.5	3.6
16.1	228	153	0.67	9.5	0.000064	0.16	20.66	0.25	0.0537	0.0009	0.0483	0.0006	304.3	3.6
17.1	291	135	0.47	12.3	0.000006	0.07	20.34	0.24	0.0531	0.0010	0.0491	0.0006	309.1	3.6
18.1	181	89	0.49	7.7	0.000472	<0.01	20.09	0.26	0.0522	0.0014	0.0498	0.0007	313.3	4.1
19.1	189	99	0.53	8.0	0.000085	0.17	20.27	0.25	0.0539	0.0010	0.0492	0.0006	309.9	3.8
20.1	212	93	0.44	8.6	0.000388	0.25	21.15	0.26	0.0543	0.0010	0.0472	0.0006	297.1	3.6
							Weighted Mean ^{206}Pb/^{238}U Age 308.5 ± 2.2 Ma							
Sample CLL-30														
1.1	287	223	0.78	9.6	0.000688	1.45	25.59	0.39	0.0627	0.0014	0.0385	0.0006	243.6	3.7
2.1	101	78	0.78	3.6	0.004070	9.31	24.23	0.64	0.1254	0.0049	0.0374	0.0011	236.9	7.1
3.1	323	105	0.32	4.6	0.004391	7.87	59.83	0.97	0.1105	0.0027	0.0154	0.0003	98.5	1.9
3.2	90	62	0.69	2.8	0.000116	1.70	27.32	0.41	0.0643	0.0025	0.0360	0.0006	227.9	3.5
5.1	116	87	0.75	3.8	0.001410	3.14	26.28	0.47	0.0759	0.0024	0.0369	0.0007	233.3	4.3
6.1	113	98	0.87	3.7	0.001460	4.23	25.91	0.47	0.0847	0.0026	0.0370	0.0007	233.9	4.4
7.1	107	103	0.96	3.6	0.002646	3.83	25.47	0.47	0.0816	0.0026	0.0378	0.0007	239.0	4.6
8.1	166	132	0.79	5.6	0.001355	1.84	25.48	0.43	0.0658	0.0018	0.0385	0.0007	243.7	4.1
9.1	65	49	0.76	2.3	0.002061	3.22	24.68	0.50	0.0769	0.0030	0.0392	0.0008	247.9	5.1
10.1	112	79	0.71	3.7	0.001488	4.12	25.67	0.46	0.0839	0.0025	0.0373	0.0007	236.4	4.5
11.1	208	241	1.16	7.0	0.001359	2.16	25.50	0.41	0.0683	0.0020	0.0384	0.0006	242.8	4.0
12.1	113	91	0.81	3.8	0.002178	2.87	25.43	0.46	0.0740	0.0023	0.0382	0.0007	241.6	4.4
13.1	66	47	0.71	2.5	0.008480	11.99	22.81	0.47	0.1471	0.0069	0.0386	0.0011	244.0	6.8
13.2	94	72	0.77	3.2	0.004291	7.13	25.25	0.47	0.1079	0.0031	0.0368	0.0008	232.9	4.9
14.1	112	77	0.69	3.8	0.002026	4.06	25.46	0.53	0.0835	0.0026	0.0377	0.0008	238.4	5.1
14.2	305	376	1.23	10.3	0.000026	0.43	25.56	0.30	0.0545	0.0008	0.0390	0.0005	246.4	2.8
15.1	186	205	1.10	6.4	0.002964	3.78	25.03	0.41	0.0813	0.0019	0.0384	0.0007	243.1	4.2
16.1	183	134	0.73	6.4	0.002875	4.96	24.66	0.41	0.0907	0.0020	0.0385	0.0007	243.8	4.3
17.1	138	101	0.73	4.9	0.003064	6.93	24.04	0.41	0.1066	0.0025	0.0387	0.0008	244.8	4.8
18.1	205	188	0.92	6.9	0.001894	3.55	25.30	0.41	0.0794	0.0022	0.0381	0.0007	241.2	4.1
19.1	87	69	0.79	2.9	0.000331	1.06	25.70	0.38	0.0596	0.0022	0.0385	0.0006	243.5	3.7
20.1	135	149	1.11	4.5	0.000657	0.55	25.60	0.40	0.0555	0.0013	0.0388	0.0006	245.7	3.8
21.1	98	73	0.75	3.3	0.000466	1.05	25.29	0.36	0.0596	0.0018	0.0391	0.0006	247.4	3.5
22.1	146	100	0.68	5.0	0.001480	2.03	25.23	0.33	0.0673	0.0038	0.0388	0.0006	245.6	3.4
23.1	139	130	0.94	4.6	0.000323	0.66	26.12	0.34	0.0563	0.0012	0.0380	0.0005	240.6	3.1
24.1	145	102	0.70	5.0	0.000146	0.32	25.23	0.33	0.0538	0.0012	0.0395	0.0005	249.8	3.2
25.1	130	110	0.84	4.5	0.000093	0.67	25.05	0.33	0.0566	0.0020	0.0397	0.0005	250.7	3.3
26.1	174	165	0.95	5.9	0.000169	0.54	25.22	0.32	0.0555	0.0011	0.0394	0.0005	249.4	3.1
28.1	77	56	0.73	2.6	0.000023	0.80	25.71	0.39	0.0575	0.0026	0.0386	0.0006	244.0	3.8
29.1	149	171	1.15	4.9	0.000128	0.67	26.06	0.34	0.0564	0.0012	0.0381	0.0005	241.1	3.1
30.1	186	152	0.82	6.4	0.000278	0.31	24.92	0.32	0.0538	0.0010	0.0400	0.0005	252.9	3.2
31.1	135	104	0.77	4.6	0.000828	0.51	25.24	0.40	0.0552	0.0017	0.0394	0.0006	249.3	3.9
32.1	143	118	0.83	4.9	0.000192	0.61	25.17	0.33	0.0561	0.0015	0.0395	0.0005	249.7	3.3
33.1	103	71	0.69	3.6	0.000466	0.60	24.63	0.47	0.0562	0.0021	0.0404	0.0008	255.1	4.9
34.1	58	42	0.73	2.0	0.000694	2.11	24.28	0.39	0.0682	0.0034	0.0403	0.0007	254.8	4.3
							Weighted Mean ^{206}Pb/^{238}U Age 244.8 ± 2.5 Ma							

Appendix B (*continued*)

							Total				Radiogenic		Age (Ma)	
Grain. spot	U (ppm)	Th (ppm)	Th/U	$^{206}Pb^*$ (ppm)	$^{204}Pb/^{206}Pb$	f_{206} %	$^{238}U/^{206}Pb$	±	$^{207}Pb/^{206}Pb$	±	$^{206}Pb/^{238}U$	±	$^{206}Pb/^{238}U$	±
Sample CLL-297														
1.1	517	456	0.88	17.6	–	<0.01	25.27	0.28	0.0506	0.0007	0.0396	0.0004	250.3	2.8
2.1	416	286	0.69	14.0	–	<0.01	25.60	0.29	0.0509	0.0013	0.0391	0.0005	247.1	2.8
3.1	395	338	0.85	13.4	–	0.04	25.42	0.29	0.0515	0.0009	0.0393	0.0005	248.7	2.8
4.1	243	164	0.68	7.9	0.000432	<0.01	26.30	0.32	0.0505	0.0010	0.0380	0.0005	240.7	2.9
							Weighted Mean $^{206}Pb/^{238}U$ Age 248.7 ± 3.3 Ma							
Sample CLL-32														
1.1	647	504	0.78	21.5	0.000536	0.44	25.888	0.375	0.0546	0.0008	0.0385	0.0006	243.3	3.5
2.1	474	431	0.91	15.7	0.000779	0.99	25.903	0.384	0.0589	0.0010	0.0382	0.0006	241.8	3.6
3.1	280	191	0.68	9.5	0.001439	1.80	25.468	0.397	0.0655	0.0014	0.0386	0.0006	243.9	3.8
4.1	453	297	0.66	15.2	0.000750	0.99	25.553	0.380	0.0590	0.0011	0.0387	0.0006	245.1	3.6
5.1	291	265	0.91	9.8	0.001709	1.30	25.569	0.396	0.0615	0.0013	0.0386	0.0006	244.2	3.8
6.1	519	400	0.77	16.7	0.000676	1.12	26.673	0.393	0.0599	0.0010	0.0371	0.0006	234.6	3.4
7.1	356	237	0.67	11.8	0.000316	0.94	26.006	0.395	0.0585	0.0012	0.0381	0.0006	241.0	3.6
8.1	523	392	0.75	17.6	0.000544	0.74	25.528	0.374	0.0570	0.0012	0.0389	0.0006	245.9	3.6
9.1	476	402	0.84	16.1	0.000419	0.60	25.386	0.374	0.0560	0.0010	0.0392	0.0006	247.6	3.6
10.1	354	269	0.76	12.1	0.000809	0.90	25.062	0.379	0.0584	0.0011	0.0395	0.0006	250.0	3.8
11.1	218	198	0.91	7.2	0.001112	2.03	25.967	0.418	0.0672	0.0016	0.0377	0.0006	238.7	3.9
12.1	184	91	0.50	7.8	0.000403	1.29	20.383	0.329	0.0628	0.0015	0.0484	0.0008	304.9	4.9
13.1	395	439	1.11	13.2	0.000520	1.34	25.667	0.384	0.0618	0.0011	0.0384	0.0006	243.1	3.6
14.1	556	571	1.03	18.7	0.000338	0.73	25.486	0.373	0.0570	0.0009	0.0390	0.0006	246.3	3.6
15.1	306	219	0.72	10.0	0.000948	1.46	26.220	0.404	0.0626	0.0013	0.0376	0.0006	237.8	3.7
16.1	514	467	0.91	17.0	0.000499	0.81	25.994	0.381	0.0575	0.0010	0.0382	0.0006	241.4	3.5
17.1	253	340	1.34	8.2	0.001219	1.37	26.437	0.415	0.0619	0.0014	0.0373	0.0006	236.1	3.7
18.1	740	801	1.08	25.1	0.000417	0.70	25.344	0.367	0.0568	0.0008	0.0392	0.0006	247.8	3.6
19.1	488	470	0.96	16.2	0.000738	1.06	25.804	0.381	0.0595	0.0012	0.0383	0.0006	242.6	3.6
20.1	258	217	0.84	8.6	0.001637	2.14	25.737	0.406	0.0682	0.0016	0.0380	0.0006	240.6	3.8
							Weighted Mean $^{206}Pb/^{238}U$ Age 243.2 ± 2.1 Ma							

Notes: (1) Uncertainties are given at the one σ level for individual spot analyses; (2) Error in FC1 reference zircon calibration for the respective analytical session was: 0.32% for samples CLL-221 y CLL-223; 0.35% for CLL-238; 0.37% for CLL-73 and CLL-75; 0.39% for CLL-44; 0.45% for CLL-76; 0.47% for CLL-85; and 0.51% for CLL-30 and CLL-32. Error in Temora reference zircon calibration was: 0.33% for CLL-114 and CLL-237; 0.34% for CLL-297 (not included in above errors, but required when comparing data from different mounts and incorporated in the mean weighted age); (3) "–" denotes that no ^{204}Pb was detected; (4) f_{206} % denotes the percentage of ^{206}Pb that is common Pb; (5) for common Pb was done using the measured $^{238}U/^{206}Pb$ and $^{207}Pb/^{206}Pb$ ratios following Tera and Wasserburg (1972), as outlined in Williams (1998; the so called ^{207}Pb correction method).

References

Baker, M.C.W., 1977. Geochronology and volcanology of Upper Cenozoic volcanic activity in north Chile and southwest Bolivia. Ph.D. Thesis, Open University, Milton Keynes, London, 249 p.

Bahlburg, H., 1993. Hypothetical southeast Pacific continent revisited: new evidence from the middle Paleozoic basins of northern Chile. Geology 21, 909–912.

Bahlburg, H., Herv́, F., 1997. eodynamic evolution and tectono-stratigraphic terranes of northwestern Argentina and northern Chile. Geological Society of America Bulletin, 109,, 869–884.

Bisso, C.B., Durán, M., Gonzales, A., 1998. Geology of the Ujina and Rosario copper porphyry deposits Collahuasi district, Chile. In: Porter, T.M. (Ed.), Porphyry and Hydrothermal Copper and Gold Deposits: A Global Perspective. PGC Publishing, Adelaide, pp. 217–232.

Black, L.P., Kamo, S.L., Allen, C.M., Aleinikoff, J.N., Davis, D.W., Korsch, R.J., Foudoulis, C., 2003. TEMORA 1: a new zircon standard for phanerozoic U–Pb geochronology. Chemical Geology 200, 155–170.

Boric, R., Díaz, F., Maksaev, V., 1990. Geología y yacimientos metalíferos de la Región de Antofagasta. Servicio Nacional de Geología y Minería. Santiago, Chile, Boletín, Vol. 40. 246.

Breitkreuz, C., Zeil, W., 1994. The Late Carboniferous to Triassic volcanic belt in Northern Chile. In: Reutter, K.J., Scheuber, E., Wigger, P.J. (Eds.), Tectonics of the Southern Central Andes. Springer, Berlin, pp. 277–292.

Brown, M., 1991. Comparative geochemical interpretation of Permian–Triassic plutonic complexes of the Coastal Range and Altiplano (23°30′ to 26°30′S), northern Chile. Geological Society of America, Special Paper 265, 157–171.

Camus, F., 2003. Geología de los Sistemas Porfíricos en los Andes de Chile. Servicio Nacional de Geología y Minería. Santiago, Chile, p. 267.

Capdevila, R., Mégard, F., Paredes, J., Vidal, P., 1977. Le Batholite de San Ramon, (Cordillère Orientale du Pérou Central) un granite tardihercynien mis en place à la limite Permien-Trias. Données géologiques et radio-métriques. Geologische Rundschau 66, 434–446.

Carlier, G., Grandin, G., Laubacher, G., Marocco, R., Megard, F., 1982. Present knowledge of the magmatic evolution of the eastern Cordillera of Peru. Earth-Science Reviews 18, 253–283.

Casquet, C., Pankhurst, R.J., Rapela, C.W., Galindo, C., Fanning, C.M., Chiaradia, M., Baldo, E., González-Casado, J.M., Dahlquist, J.A., 2007. The Mesoproterozoic Maz terrane in the Western Sierras Pampeanas, Argentina, equivalent to the Arequipa–Antofalla block of southern Peru? Implications for West Gondwana margin evolution. Gondwana Research. doi:10.1016/j.gr.2007.04.005.

Chew, D.M., Schaltegger, U., Košler, J., Whitehouse, M.J., Gutjahr, M., Spikings, R.A., Mišković, A., 2007. U–Pb geochronologic evidence for the evolution of the Gondwanan margin of the north-central Andes. GSA Bulletin 119, 697–711.

Chu, N-C., Taylor, R.N., Chavagnac, V., Nesbitt, R.W., Boella, R.M., Milton, J.A, German, C.J., Bayon, G., Burton, K., 2002. Hf isotope ratio analysis using multi-collector inductively coupled plasma mass spectrometry: an evaluation of isobaric interference corrections. Journal of Analytical Atomic Spectrometry 17, 1567–1574.

Cornejo, P., Mpodozis, C., Tomlinson, A.J., 1998. Hoja Salar de Maricunga, Región de Atacama. Servicio Nacional de Geología y Minería (SERNA-GEOMIN), Santiago, Chile, Mapas Geológicos 1:100.000, no. 7.

Cornejo, P., Matthews, S., Marinovic, N., Pérez de Arce, C., Basso, M., Alfaro, J., Navarro, M., 2006. Alteración hidrotermal y mineralización recurrente de Cu y Cu–Mo durante el Pérmico y el Triásico en la Cordillera de Domeyko (Zona de Zaldívar-Salar de los Morros): antecedentes geocronológicos U–Pb, $^{40}Ar/^{39}Ar$ y Re–Os. XI Congreso Geológico Chileno 2, 219–222.

Damm, K.-W., Pichowiak, S., Todt, W., 1986. Geochemie, petrologie und geochronologie der plutonite und des metamorphen grundgebirges in nordchile. Berliner Geowissenschaftliche Abhandlungen (A) 66, 73–146.

Eggins, S.M., 2003. Laser ablation ICP-MS analysis of geological materials as lithiumborate glasses. Geostandards Newsletter: The Journal of Geostandards and Geoanalysis 27, 147–162.

Eggins, S.M., Grün, R., McCulloch, M.T., Pike, A.W.G., Chappell, J., Kinsley, L., Mortimer, G., Shelley, M., Murray-Wallace, C.V., Spötl, C., Taylor, L., 2005. In situ U-series dating by laser-ablation multi-collector ICPMS; new prospects for Quaternary geochronology. Quaternary Science Reviews 24, 2523–2538.

Franz, G., Lucassen, F., Kramer, W., Trumbull, R.B., Romer, R.L., Wilke, H.-G., Viramonte, J.G., Becchio, R., Siebel, W., 2006. Crustal evolution at the Central Andean continental margin: a geochemical record of crustal growth, recycling and destruction-. In: Oncken, O., Chong, G., Franz, G., Giese, P., Götze, H.-J., Ramos, V., Strecker, M.R., Wigger, P. (Eds.), The Andes-Active Subduction Orogeny. Springer, pp. 45–64.

Galli, C., 1968. Cuadrángulo Juan de Morales, Provincia de Tarapacá. Instituto de Investigaciones Geológicas, Carta Geológica de Chile, 1:50.000, 18, 53 p.

García, F. 1967. Geología del Norte Grande de Chile. Sociedad Geológica de Chile, Santiago, Simposio sobre el Geosinclinal Andino, Publicación 3.

Huete, C., Maksaev, V., Moscoso, R., Ulriksen, C., Vergara, H., 1977. Antecedentes geocronológicos de rocas intrusivas y volcánicas en la Cordillera de los Andes comprendida entre la Sierra de Moreno y el río Loa y los 21° y 22° Lat. Sur, II Región, Chile. Revista Geológica de Chile 4, 35–41.

Iriarte, S., Arévalo, C., Mpodozis, C., Rivera, O. 1996. Mapa Geológico de la Hoja Carrera Pinto, Región de Atacama. Servicio Nacional de Geología y Minería, Santiago, Mapas Geológicos 3, escala 1.100.000.

Lancelot, J.R., Laubacher, G., Marocco, R., Renaud, U., 1978. U/Pb radiochronology of two granitic plutons from the eastern Cordillera (Peru) — extent of Permian magmatic activity and consequences. Geologische Rundschau 67, 236–243.

Llambías, E.J., Sato, A.M., 1990. El Batolito de Colangüil, Cordillera Frontal, Argentina: Estructura y marco tectónico. Revista Geológica de Chile 17, 89–108.

Llambías, E.J., Kleiman, L.E., Salvarredi, J.A., 1993. El Magmatismo Gondwánico. In: Ramos, V. (Ed.), Geología y Recursos Naturales de Mendoza, Relatorio, XII Congreso Geológico Argentino y II Congreso de Exploración de Hidrocarburos (Mendoza), pp. 53–64.

Llambías, E.J., Sato, A.M., 1995. El Batolito de Colangüil: transición entre orogénesis y anorogénesis. Revista de la Asociación Geológica Argentina, Buenos Aires 50 (1–4), 111–131.

Lucassen, F., Franz, G., Thirlwall, M.F., Mezger, K., 1999. Crustal recycling of metamorphic basement, Late Paleozoic granitoids of northern Chile (~22°S): implications for the composition of the Andean crust. Journal of Petrology 40, 1527–1551.

Ludwig, K.R., 2001. SQUID 1.02, A User's Manual; Berkeley Geochronology Center Special Publication. No. 2, 2455 Ridge Road, Berkeley, CA 94709, USA.

Ludwig, K.R., 2003. User's Manual for Isoplot/Ex, Version 3.0, A Geochronological Toolkit for Microsoft Excel. Berkeley Geochronology Center Special Publication No. 4, 2455 Ridge Road, Berkeley CA 94709, USA.

Maksaev, V., 1990. Metallogeny, geological evolution, and thermochronology of the Chilean Andes between latitudes 21° and 26° south, and the origin of major porphyry copper deposits: Ph.D. Thesis, Dalhousie University, Halifax, N.S., Canada, 554 p.

Maksaev, V., Munizaga, F., Giglio, S., 2006. Low Temperature Thermochronology of the Collahuasi Porphyry Copper District. V South American Symposium on Isotope Geology, Punta del Este, Uruguay, p. 517.

Marinovic, N., Lahsen, A., 1984. Hoja Calama. Servicio Nacional de Geología y Minería. Santiago, Carta Geológica de Chile 58.

Marinovic, N. and García, M. 1999. Hoja Pampa Unión. Región de Antofagasta. Servicio Nacional de Geología y Minería, Santiago, Mapas Geologicos, 9, escala 1:100.000.

Marinovic, N., Smoje, I., Maksaev, V., Hervé, M., Mpodozis, C., 1995. Hoja Aguas Blancas, Región de Antofagasta. Servicio Nacional de Geología y Minería. Santiago, Carta Geológica de Chile 70.

Martin, M., Clavero, J., Mpodozis, C., 1999. Late Paleozoic to Early Jurassic tectonic development of the high Andean Principal Cordillera, El Indio Region, Chile (29–30°S). Journal of South American Earth Sciences 12, 33–40.

Masterman, G.L., 2003. Structural and geochemical evolution of the Rosario Copper — molybdenum porphyry deposit and related copper veins, Collahuasi District, Northern Chile. Ph.D. Thesis, University of Tasmania, Australia, 253 p.

Masterman, G.J., Cooke, D.R., Berry, R.F., Clark, A.H., Archibald, D.A., Mathur, R., Walshe, J.L., Duran, M., 2004. $^{40}Ar/^{39}Ar$ and Re–Os geochronology of porphyry copper–molybdenum deposits and related copper–silver veins in the Collahuasi district, northern Chile. Economic Geology 99, 673–690.

Masterman, G.J., Cooke, D.R., Berry, R.F., Walshe, J.L., Lee, A.W., Clark, A.H., 2005. Fluid chemistry, structural setting, and emplacement history of the Rosario Cu–Mo porphyry and Cu–Ag–Au epithermal veins, Collahuasi District, Northern Chile. Economic Geology 100, 835–862.

Mercado, M. 1982. Hoja Laguna del Negro Francisco, Región de Atacama. Servicio Nacional de Geología y Minería, Santiago, Carta Geológica de Chile, 56, escala 1:100.000.

Miskovic, A., Schaltegger, U., 2006. Magmatic trends along the Peruvian Cordillera Oriental — probing the evolution of the proto-Andean accretionary margin. Geophysical Research Abstracts, v. 8, 02028. European Geosciences Union.

Mpodozis, C., Kay, S.M., 1990. Provincias magmáticas ácidas y evolución tectónica de Gondwana, Andes Chilenos (28–31°S). Revista Geológica de Chile 17, 153–180.

Mpodozis, C., Kay, S., 1992. Late Paleozoic to Triassic evolution of the pacific Gondwana margin: evidence from Chilean frontal Cordilleran batholiths. Geological Society of America Bulletin 104, 999–1014.

Nasi, C., Mpodozis, C., Cornejo, P., Moscoso, R., Maksaev, V., 1985. El Batolito Elqui-Limarí (Paleozoico Superior-Triásico): características petrográficas, geoquímicas y significado tectónico. Revista Geológica de Chile 25–26, 77–111.

Patchett, P.J., Kouvo, O., Hedge, C.E., Tatsumoto, M., 1981. Evolution of continental crust and mantle heterogeneity: evidence from Hf isotopes. Contributions to Mineralogy and Petrology 78, 279–297.

Ramos, V.A., 1988. Late Proterozoic–Early Paleozoic of South America— a collisional history. Episodes 11, 168–174.

Rolleri, E.O., Criado Roque, P., 1970. Geología de la provincia de Mendoza. IV Jornadas Geológicas Argentinas (Mendoza, 1969). Actas, Asociación Geológica Argentina, Buenos Aires 2, 1–60.

Sato, A.M., Llambías, E.J., 1993. El Grupo Choiyoi, provincia de San Juan: equivalente del Batolito de Colangüil. XII Congreso Geológico Argentino Actas. Asociación Geológica Argentina, Buenos Aires 4, 156–165.

Schaltegger, U., Chew, D., Miskovic, A., 2006. Neoproterozoic to Early Mesozoic evolution of the Western Gondwana margin: evidence from the eastern Cordillera of Peru. Abstract, XIII. Congreso Peruano de Geología, Lima 17–20 October.

Skarmeta, J., Marinovic, N., 1981. Hoja Quillagua, Región de Antofagasta. Instituto de Investigaciones Geológicas. Carta Geológica de Chile 51, 63 p.

Steiger, R.H., Jäger, E., 1977. Subcommission on geochronology: convention on the use of decay constants in geo- and cosmochronology. Earth and Planetary Science Letters 36, 359–362.

Strazzere, L., Daniel, A., Gregori, D.A., Dristas, J.A., 2006. Genetic evolution of Permo-Triassic volcaniclastic sequences at Uspallata, Mendoza Precordillera, Argentina. Gondwana Research 9, 485–499.

Tassinari, C.C.G., Medina, J.G., Pinto, S.M., 1996. Rb–Sr and Sm–Nd geochronology and isotope geochemistry of Central Iberian metassedimentary rocks (Portugal). Geologie en Mijnbouw 75, 69–79.

Taylor, S.R., McLennan, S.M., 1985. The Continental Crust: Its Composition and Evolution. Blackwell Scientific, Oxford. 312 p.

Tera, F., Wasserburg, G., 1972. U–Th–Pb systematics in three Apollo 14 basalts and the problem of initial Pb in lunar rocks. Earth and Planetary Science Letters 14, 281–304.

Thirlwall, M.F., Anczkiewicz, R., 2004. Multidynamic isotope ratio analysis using MC-ICP-MS and the causes of secular drift in Hf, Nd and Pb isotope ratios. International Journal of Mass Spectrometry 235, 59–81.

Tomlinson, A.J., Cornejo, P., Mpodozis, C., 1999. Hoja Potrerillos, Región de Atacama, SERNAGEOMIN, Mapas Geológicos, 14, escala 1:100.000.

Tomlinson, A.J., Blanco, N., Maksaev, V., Dilles, J.H., Grunder, A.L., Ladino, M., 2001. Geología de la Precordillera Andina de Quebrada Blanca-Chuquicamata, Regiones I y II (20°30′–22°30′ S). Servicio Nacional de Geología y Minería — Corporación del Cobre de Chile, SERNAGEOMIN Informe Registrado, IR-01-20. 444 p.

Vaughan, A.P.M., Pankhurst, R.J., 2007. Tectonic overview of the West Gondwana margin. Gondwana Research. doi:10.1016/j.gr.2007.07.004.

Vergara, H., 1978. Cuadrángulo Ujina, Región de Tarapacá, Instituto de Investigaciones Geológicas, Carta Geológica de Chile, 33, 63 p., escala 1:50.000.

Vergara, H., Thomas, A., 1984. Hoja Collacagua, Región de Tarapacá, Servicio Nacional de Geología y Minería, Carta Geológica de Chile, 59, 79 p., escala 1:250.000.

Vervoort, J.D., Blichert-Toft, J., 1999. Evolution of the depleted mantle: Hf isotope evidence from juvenile rocks through time. Geochimica et Cosmochimica Acta 63, 533–556.

Vinasco, C.J., Cordani, U.G., González, H., Weber, M., Pelaez, G., 2006. Geochronological, isotopic, and geochemical data from Permo-Triassic granitic gneisses and granitoids of the Colombian Central Andes. Journal of South American Earth Sciences 21, 355–371.

Williams, I.S., 1998. U–Th–Pb geochronology by ion microprobe. In: McKibben, M.A., Shanks III, W.C., Ridley, W.I. (Eds.), Applications of Microanalytical Techniques to Understanding Mineralizing Processes. Reviews in Economic Geology, 7, pp. 1–35.

Zhang, S.H., Zhao, Y., Song, B., Yang, Y.H., 2007. Zircon SHRIMP U–Pb and in-situ Lu–Hf isotope analyses of a tuff from Western Beijing: evidence for missing Late Paleozoic arc volcano eruptions at the northern margin of the North China block. Gondwana Research 12, 157–165.